Chapter 6

Mantle Convection with Strong Subduction Zones

Abstract. Because mantle viscosity is temperature-dependent, cold subducting lithosphere should be strong, which implies that the rapid, localized deformation associated with subduction should resist plate motions, and thus slow convection in the underlying mantle. Due to computational constraints, the deformation of a subducting plate cannot be accurately resolved in mantle-scale convection models, so its affect on convection is difficult to investigate. We have developed a new method for implementing subduction that parameterizes the deformation associated with bending of the oceanic lithosphere within a small region of a finite element grid. By imposing velocity boundary conditions in the vicinity of the subduction zone, we enforce a geometry for subduction, producing a slab with a realistic thermal structure. To make the model dynamically consistent, we specify a rate for subduction that balances the energy budget for convection, which includes an expression for the energy needed to bend the oceanic lithosphere as it subducts. This expression is determined from a local model of bending for a strong viscous slab. By implementing subduction in this way, we have demonstrated convection with plates and slabs that resemble those observed on Earth, but in which up to 30% of the mantle's total convective resistance is associated with deformation occurring within the subduction zone. This additional resistance slows plate velocities by nearly a factor of two compared to models with

a weak slab. For sufficiently strong lithosphere, the bending deformation is sufficient to stop plate motions altogether and causes convection beneath a "stagnant lid." By introducing a low-viscosity asthenosphere beneath the oceanic plate, we demonstrate that small-scale convection at the base of oceanic lithosphere may limit plate thickness, and thus the resistance to bending, and causes plate velocities to depend on the strength of the bending lithosphere rather than on the viscosity of the underlying mantle. For a cooling Earth, lithospheric strength should be nearly constant, but the mantle viscosity should increase with time. Thus, subduction-resisted convection should produce nearly constant plate velocities and heat flow over time, which has implications for the thermal evolution of the Earth. We estimate that this style of convection should apply for the Earth if the effective viscosity of the bending lithosphere is greater than about 10^{23} Pa s, but only if some mechanism, such as small-scale convection, prevents the bending resistance from stopping plates altogether. Such a mechanism could be fundamental to plate tectonics and Earth's thermal history.

6.1   Introduction

The motions of Earth's tectonic plates are understood to be the surface expression of convection in the mantle. Because the plates are cold, they are denser than the mantle beneath them, and thus gravitationally unstable. For Earth, this instability manifests itself as subduction, in which oceanic lithosphere bends and dives into the mantle beneath overriding plates. Because it involves the entire oceanic lithosphere, subduction is an efficient mechanism for converting the significant negative buoyancy of the surface plates into horizontal density gradients that drive convection. In fact, subducted lithosphere is thought to drive plate motions, and thus mantle-scale flow, by pulling on attached surface plates [e.g., *Chapple and Tullis*, 1977; *Forsyth and Uyeda*, 1975; *Hager and O'Connell*, 1981; *Lithgow-Bertelloni and Richards*, 1995].

The cold temperatures of surface plates also make them stiffer than the underlying mantle, a fact that causes plates to move rigidly as coherent units. The temperature-dependent viscosity that strengthens plate interiors, however, should also strengthen

subducting lithosphere, and thus tend to resist the rapid localized deformation associated with subduction. Indeed, numerical studies of mantle convection show that if temperature-induced viscosity contrasts are above about $10^3 - 10^5$, a cold thermal boundary layer can become strong enough to resist deformation altogether, forcing convection to occur instead beneath a "stagnant lid" [e.g., *Christensen*, 1984a; *Davaille and Jaupart*, 1993; *Moresi and Solomatov*, 1995; *Ratcliff et al.*, 1997; *Solomatov*, 1995]. Laboratory measurements of the temperature-dependence of diffusion or dislocation creep in mantle rocks [e.g., *Hirth and Kohlstedt*, 1996; *Karato et al.*, 1986] suggest an order of magnitude variation in viscosity for every 100°C degrees of temperature change. For a temperature difference of $\sim 600^{\circ}$C across the ductile part of the lithosphere, viscosity variations should be more than sufficient for a stagnant lid to develop, yet this style of convection is not dominant for Earth. Subduction zones, then, serve to break an otherwise stagnant lid by permitting the rapid localized deformation that is required for plate-like motions to occur. The weakening mechanism that allows subduction is not well understood, but brittle fracture [e.g., *Moresi and Solomatov*, 1998; *Zhong and Gurnis*, 1996; *Zhong et al.*, 1998], strain-rate-weakening [e.g., *Tackley*, 1998], a maximum yield stress [e.g., *Trompert and Hansen*, 1998], and various self-lubricating rheologies [e.g., *Bercovici*, 1996; 1998; *Lenardic and Kaula*, 1994] have been proposed as possibilities.

Generating plate-like behavior in numerical models of mantle convection generally involves weakening convergent plate boundaries in some way, and justifying this action by appealing to one or more of the above mechanisms for weakening. For example, one commonly-used method is to simply parameterize all of the possible weakening effects into low-viscosity "weak zones" that are imposed between high-viscosity plates [e.g., *Davies*, 1989; *Gurnis and Hager*, 1988; *King and Hager*, 1990; 1994; *Puster et al.*, 1995]. Weak zones also can be generated naturally by applying stress-weakening or self-lubricating constitutive laws to the lithosphere. This generates "instantaneous" zones of weakness between rigid plates and avoids the necessity of imposing plate boundary locations [e.g., *Bercovici*, 1996; 1998; *Lenardic and Kaula*, 1994; *Tackley*, 1998; *Trompert and Hansen*, 1998]. Other studies break the surface lithosphere with

a fault that allows a jump in velocity across its width and may support some degree of shear stress [e.g., *Toth and Gurnis*, 1998; *Zhong and Gurnis*, 1994, 1995a, b; *Zhong et al.*, 1998]. Finally, plate-like behavior can be forced by simply imposing piecewise continuous plate velocities at the surface [e.g., *Hager and O'Connell*, 1979; *Davies*, 1988; *Bunge and Richards*, 1996]. Such kinematic models avoid the difficulties of implementing realistic subductions zones, but are not dynamically self-consistent.

Due to computational constraints, the deformation associated with convergent plate boundaries typically spans only a few elements of a regularly spaced finite element grid. Thus, for the above methods to be accurate, they must include the deformation of a subducting plate within the small region of weakening in which subduction is implemented. It is not clear, however, that any of these studies achieve an accurate representation of subduction because the convergence that occurs in these studies is not compared to detailed observations available at subduction zones. For example, the seismicity of the upper 200 km of Wadati-Benioff zones is thought to indicate plate bending as a slab begins to subduct, followed by unbending as the straightens and continues into the mantle [e.g., *Bevis*, 1986; 1988; *Engdahl and Scholz*, 1977; *Hasegawa et al.*, 1994; *Isacks and Barazangi*, 1977; *Kawakatsu*, 1986]. This unique strain pattern has been reproduced in detailed local models of subduction [e.g., *Conrad and Hager*, 1999a; *Houseman and Gubbins*, 1997; *Melosh and Raefsky*, 1980; *Toth and Gurnis*, 1998; *Zhang et al.*, 1985] in which a strong plate is forced to bend as it passes through a realistic subduction zone geometry. Global-scale models must parameterize subduction more coarsely and thus cannot accurately mimic the stresses associated with bending or unbending within the subducting plate.

Part of the deformation that occurs during subduction is expressed as brittle fracture by seismicity. Brittle fracture is an inelastic deformation mechanism, which means that energy is dissipated as the subducting plate bends and unbends in the subduction zone [e.g., *Chapple and Forsyth*, 1979]. In addition, the mantle certainly behaves as a highly temperature-dependent fluid, so additional inelastic deformation should occur as viscous flow. Thus, subduction zones may demand a significant fraction of the mantle's total energy budget. In fact, *Conrad and Hager* [1999a] show

that if slabs remain two orders of magnitude stronger than the upper mantle as they descend, the bending and unbending of oceanic lithosphere at subduction zones may require as much energy as viscous flow within the mantle interior. If the energy spent on plate bending were available instead for deforming the mantle, as it would be if subduction zones were weak, significantly faster plate velocities would result. Thus, it is possible that plate bending at subduction zones, by retarding the flow of the oceanic lithosphere into the mantle interior, could limit plate velocities. This result is confirmed by *Becker et al.* [1999], who compare laboratory and numerical experiments for a growing slab.

Because most large-scale convection models requires convergent plate boundaries to be weak for subduction to occur, the energy dissipated at these boundaries should not be particularly large. On the other hand, *Conrad and Hager's* [1999a] local model of subduction produces plate-like behavior while dissipating significant energy within a subducting slab that remains strong as it deforms. *Conrad and Hager's* [1999a] subduction model, however, uses an irregular finite element grid that is both too complicated and of too high resolution to be of practical use in larger, mantle-scale studies. In this work, we devise a method for including the results of *Conrad and Hager's* [1999a] analysis within a small region of a large, regularly-spaced, finite element grid. To do this, we impose a geometry for subduction that produces realistic temperature and velocity fields for the resulting slab. To make subduction dynamically self-consistent, we also specify the rate at which subduction occurs by applying *Conrad and Hager's* [1999a] energy balance analysis. This method allows us to control how much energy is dissipated within the subduction zone, and thus parameterizes the effects of deformation within the subduction zone on convection in the entire mantle. Using this method, we study mantle convection with subduction zones that dissipate a significant fraction of the mantle's convective energy, as they should if oceanic plates remain strong as they subduct. In doing so, we determine the maximum amount of bending dissipation that is possible before "stagnant lid" convection develops. In addition, we confirm some of the predictions made by *Conrad and Hager* [1999b], who suggest that the bending resistance at subduction zones

could profoundly influence Earth's thermal history.

6.2 The Energetics of Mantle and Lithosphere Deformation

Convection in the mantle is typically formulated as a balance between viscous stresses and gravitational body forces, but it can also be described by an energy balance between the rate at which gravitational potential energy is released and the rate at which this energy is dissipated viscously by the deformation of mantle and lithosphere materials [e.g., *Backus*, 1975; *Chandrasekhar*, 1961, pp. 12-14; *Conrad and Hager*; 1999a, *Hewitt et al.*, 1975]. For this study, we implement subduction-driven convection using both approaches; we use a force balance to determine viscous flow within the mantle and an energy balance to describe the effects of subduction zone deformation on the entire convecting system. More specifically, we use an expression for the energy required to bend subducting lithosphere to parameterize the gross effects of this deformation on convection, but without requiring sufficient resolution to accurately describe plate bending. To implement this energy balance, we must first determine the energy dissipated by a subducting slab and compare this to the total energy requirements of convection. Here we follow the analysis of *Conrad and Hager* [1999a], who assume a viscous rheology for the bending lithosphere. The approach, however, is general and dissipation associated with other deformation mechanisms could be included, if desired.

Mantle convection is driven by lateral variations in the mantle's heterogeneous density field. Potential energy is released largely by the downward motion of cold slabs and the upward motion of hot plumes. The total potential energy release, Φ^{pe}, can be written as:

$$\Phi^{\mathrm{pe}} = \int_A \rho g \alpha T(x,z) v_z(x,z) dA \qquad (6.1)$$

where ρ is density, g is the acceleration due to gravity, α is the thermal expansivity, T is temperature, and v_z is the vertical velocity (positive upwards). For two-dimensional

flow, the total potential energy release is calculated by integrating over the entire area, A, of the convecting system, and is given per unit length perpendicular to the plane of flow. For flow driven by the negative buoyancy of slabs, *Conrad and Hager* [1999a] show that this expression becomes:

$$\Phi^{\text{pe}} = \frac{\rho g \alpha (T_{int} - T_s) l_s h_s}{\sqrt{\pi}} v_p = C^{\text{pe}} v_p \tag{6.2}$$

where T_{int} and T_s are the temperatures of the mantle interior and surface, h_s is the thickness of the slab as it subducts, l_s is the length of the subducted portion of the slab, and v_p is the slab's downward velocity, which we assume is equal to the velocity of the attached surface plate. Here we introduce the quantity C^{pe}, which will prove useful later, to express the dependence of Φ^{pe} on everything except for v_p.

The release of potential energy is balanced by energy dissipation throughout the entire convecting system. For viscous flow, the viscous dissipation, Φ^{vd}, can be written as [e.g., *Chandrasekhar*, 1961, pp. 12-14]:

$$\Phi^{\text{vd}} = \int_A \tau_{ij} \dot{\epsilon}_{ij} dA = 2 \int_A \eta \dot{\epsilon}_{ij} \dot{\epsilon}_{ij} dA \tag{6.3}$$

where the strain-rate, $\dot{\epsilon}_{ij}$, is given by:

$$\dot{\epsilon}_{ij} = \frac{1}{2} \left(\frac{\partial u_i}{\partial x_j} + \frac{\partial u_j}{\partial x_i} \right) \tag{6.4}$$

and is related to the deviatoric stress, τ_{ij}, by the constitutive relation:

$$\tau_{ij} = 2\eta \dot{\epsilon}_{ij} \tag{6.5}$$

which defines the effective viscosity, η, of the fluid. For mantle flow driven by the motion of a plate and a slab, each moving with speed v_p, the total viscous dissipation can be expressed using (6.3) as:

$$\Phi_m^{\text{vd}} = C_m \eta_m v_p^2 \tag{6.6}$$

where η_m is the effective mantle viscosity and C_m is a geometrical constant that depends on the pattern of flow [*Conrad and Hager*, 1999a].

Because their viscosity is temperature-dependent, subducting slabs should have a material strength, expressed here as an effective viscosity η_l, that is greater than that of the underlying mantle. In addition, subduction zones accommodate large changes in surface velocity over short horizontal distances, which implies large strain-rates. According to (6.3), both of these facts indicate that the viscous dissipation for a subduction zone should be large. By combining theory with numerical calculations, *Conrad and Hager* [1999a] show that the bending and unbending of an effectively viscous lithosphere in a subduction zone produces a viscous dissipation, Φ_l^{vd}, of:

$$\Phi_l^{\mathrm{vd}} = 2v_p^2 \eta_l \left(\frac{h_s}{R} \right)^3 \tag{6.7}$$

where R is the radius of curvature that describes the bent shape of the slab. *Conrad and Hager* [1999a] show that Φ_l^{vd} may be larger than Φ_m^{vd} if the effective lithosphere viscosity is of order 10^{23} Pa s, which is only about two orders of magnitude larger than estimates for the viscosity of the underlying mantle. Significant energy dissipation may also be associated with other aspects of the subduction zone. For example, *Conrad and Hager* [1999a] estimate that dissipation in the fault zone between the slab and the overriding plate may account for up to 10% of the mantle's total energy dissipation. Additional dissipation may result from corner flow in the mantle associated with the motion of the subducting plate.

The effective lithosphere viscosity, η_l, that applies in (6.7) represents the combined effects of all of the deformation mechanisms that contribute to bending of the lithosphere, which should include viscous flow, brittle fracture, and non-Newtonian or plastic deformation. In using (6.7) to express the bending dissipation, an assumption is made that η_l does not vary with either the plate velocity v_p or the plate thickness h_s. If, however, the viscosity depends on stress or strain-rate, then η_l should decrease as either of these quantities increase. For example, if the lithosphere's brittle rheology causes it to fail for stresses above some maximum yield stress, then (6.3) suggests that

194

Φ_l^{yd} should be linearly dependent on v_p. Similarly, bending stresses should increase as h_s increases, meaning that stress-weakening should cause the effective viscosity η_l to be smaller for thicker plates. In this analysis, we study how one model for subduction zone deformation affects mantle-scale convection, using (6.7) to express bending for a viscous lithosphere. In doing so, we recognize that non-linear viscosity or subduction zone deformation not associated with bending may introduce additional behavior, but save the analysis of these complicating effects for future study.

6.3   Including Plate Bending within a Numerical Convection Calculation

To simulate the bending of oceanic lithosphere in a subduction zone, we modify ConMan, a finite element code that solves the coupled thermal diffusion and incompressible Navier-Stokes equations for a highly viscous fluid [*King et al.*, 1990]. These modifications allow the effects of plate bending to be included within a small region of a regular finite element grid. To illustrate this, we set up a finite element grid (Figure 6.1) with aspect ratio 2.5, a resolution of 40 by 100 elements, free-slip boundary conditions on the top and bottom surfaces, and flow-through boundary conditions on the two sides. Temperature boundary conditions maintain constant temperatures T_b at the grid base and $T_s < T_b$ at the surface. The surface also includes an explicitly strong continental lithosphere (40 elements wide) and oceanic lithosphere that is distinguished from the underlying mantle by its lower temperature. Temperature-dependent viscosity makes the oceanic lithosphere strong and thus causes its motions to be plate-like. The oceanic lithosphere is bounded on one side by a low-viscosity "ridge," and on the other side by a specially-designed "subduction zone" that implements the descent of oceanic lithosphere into the mantle and expresses the energy requirements of a bending plate, as described below.
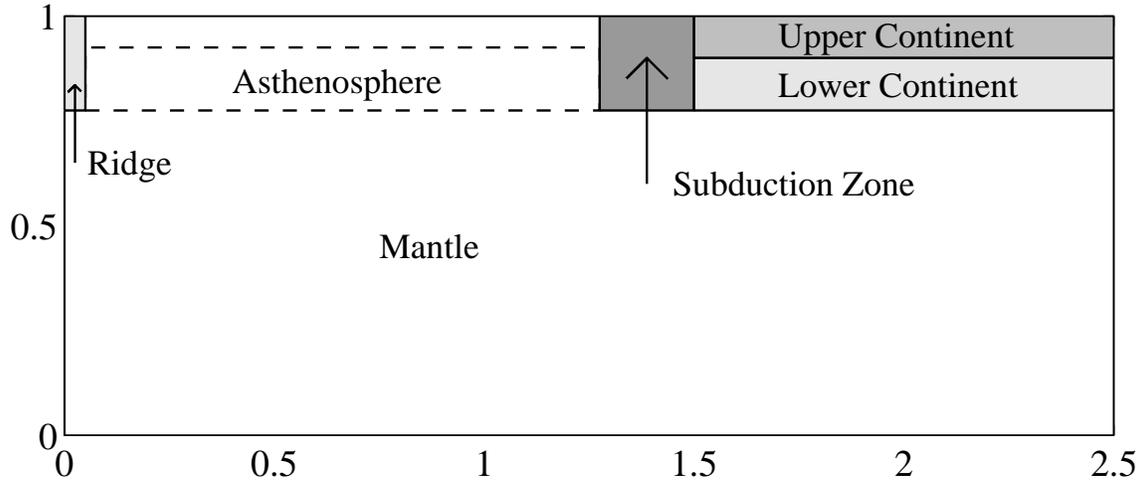
Figure 6.1: Cartoon showing the various regions of the finite element grid, each of which is characterized by different viscosity laws, as defined in Table 6.1. Mantle and subduction zone viscosity is temperature-dependent while the other regions have constant viscosity. Of these, the ridge is weak, the upper continent is strong, and the lower continent viscosity is approximately equal to that of the mantle interior. A few models include a low-viscosity asthenosphere that has a constant viscosity $1/10^{\text{th}}$ that of the mantle interior. The subduction zone region includes a set of specially-designed velocity boundary conditions (detailed in Figure 6.2) that impose the geometry for subduction.

6.3.1 Nondimensionalization

At this point, it is useful to define a set of dimensionless variables. We define the Rayleigh number, Ra_m, for the convecting system as:

$$Ra_m = \frac{\rho g \alpha \Delta T D^3}{\kappa \eta_m} \tag{6.8}$$

where ΔT is the temperature difference $T_b - T_s$, D and κ are the thickness and thermal diffusivity of the mantle layer, and η_m is its average viscosity, which in these calculations is calculated by following *Parmentier et al.* [1976], who suggest weighting the viscosity by the square of the strain-rate. We define a dimensionless viscosity, η', as:

$$\eta' = \frac{\eta}{\eta_0} \tag{6.9}$$

196

where η_0 is the mantle viscosity corresponding to $Ra_m = 10^6$, a value we use as a reference model in the calculations to follow. In these calculations, we vary Ra_m by changing η_m and keep the other terms in the Rayleigh number, as defined by (6.8), constant. We define a dimensionless temperature, T', according to:

$$T' = \frac{T - T_s}{T_b - T_s} \tag{6.10}$$

Thus, $T' = 0$ at the surface and $T' = 1$ at the base. Finally, we nondimensionalize time and distance according to:

$$t' = t\frac{\kappa}{D^2} \qquad \text{and} \qquad x' = \frac{x}{D} \tag{6.11}$$

which implies a nondimensionalization for velocity of:

$$v' = v\frac{D}{\kappa} \tag{6.12}$$

6.3.2 Viscosity Structure

The various regions of the finite element grid are distinguished by viscosity (Table 6.1). For the mantle and the subduction zone regions, viscosity is temperature-dependent, which generates plate-like flow at the surface. We use the viscosity law [e.g., *Kohlstedt et al.*, 1995]:

$$\eta'_m(T') = \eta'_m(T'_{int}) \exp\left(\frac{E_a}{RT'\Delta T} - \frac{E_a}{RT'_{int}\Delta T}\right) \tag{6.13}$$

where E_a is an activation energy, $R = 8.31$ J mol^{-1} K^{-1} is the universal gas constant, and we assume a non-adiabatic temperature variation between $T_s = 0°$C at the surface and $T_b = 2000°$C at the core-mantle boundary. We choose an initial interior temperature of $T_{int} = 1300°$C, which is a reasonable value for the Earth. This corresponds to a dimensionless value of $T'_{int} = 0.65$, which is close to the steady-state interior temperatures that are produced in this study. We choose an activation energy of $E_a = 100$ kJ mol^{-1} because this value is large enough to produce plates and slabs that move as coherent units, but weak enough to prevent the entire mantle

197

Table 6.1. Viscosity Variations within the Finite Element Model

Region	Dimensionless Viscosity[a]
Mantle[b]	$\eta'_m(T') \;=\; \eta'_m(T'_{int}) \exp\left(\frac{E_a}{RT'\Delta T} - \frac{E_a}{RT'_{int}\Delta T}\right)$
Subduction Zone[b]	$\eta'_{sz}(T') \;=\; \eta'_m(T')$
Ridge	$\eta'_r \;=\; \eta'_m(T' = 1)$
Upper Continent	$\eta'_{uc} \;=\; 1000$
Lower Continent	$\eta'_{lc} \;=\; \eta'_m(T'_{int})$
Asthenosphere[c]	$\eta'_{as} \;=\; \eta'_m(T'_{int})/10$
"Weak Zone"[c]	$\eta'_{wz} \;=\; \eta'_m(T'_{int})$

[a]Viscosity is made dimensionless using (9).

[b]Temperature-dependent viscosity is described by (13), where $T'_{int} = 0.65$ and a maximum value of $\eta' = 1000$ is enforced.

[c]The asthenosphere and the weak zone are only included in a few specific models (see text).

from evolving into a cold, immobile state. The value of $\eta'_m(T'_{int})$ is varied to produce different mantle Rayleigh numbers, Ra_m. The interior viscosity typically decreases slightly over time because the mantle interior warms to temperatures greater than $T'_{int} = 0.65$, increasing Ra_m. Finally, we set a maximum viscosity of $\eta'_{max} = 1000$ for all runs. This prevents the extremely large viscosities inherent to (6.13) at $T' = 0$, but also maintains a high constant viscosity at the surface that is not dependent on the interior viscosity. This feature is useful in an application to the thermal evolution of the Earth.

The other various regions of the finite element grid (Figure 6.1) have Newtonian viscosity that does not depend on temperature (Table 6.1). The "ridge" is a region 2 elements wide and 9 deep that has a low viscosity of $\eta'_r = \eta'_m(T' = 1)$. The weakness of the ridge allows the oceanic plate to easily pull away from the continent. The

continent itself is divided into two regions. The upper part (4 elements deep) has a strong viscosity equal to $\eta'_{uc} = 1000$, and is thus as strong as the strongest oceanic lithosphere. The lower continent (5 elements deep) has a viscosity of $\eta'_{lc} = \eta'_m(T'_{int})$, which is close to the viscosity of the mantle interior. We found it necessary to remove the temperature-dependence of fluid below the lower continent to prevent this material from cooling and then accreting to the continental base, making it overly-thick. Later, we study the effects of a low-viscosity asthenosphere beneath the oceanic plate, by applying a constant viscosity of $\eta'_{as} = \eta'_m(T'_{int})/10$ to the 4th through 9th elements from the surface, between the ridge and the subduction zone.

6.3.3   The Subduction Zone

To implement subduction, we apply velocity boundary conditions within, and on the boundaries of, the subduction zone region (Figure 6.2). On the left-hand edge of the subduction zone, an imposed horizontal velocity of magnitude v_i forces the oceanic plate into the subduction zone. This material is later forced out of the subduction zone base by boundary conditions that impose vertical velocity of magnitude v_i. Within the subduction zone, the fluid is forced to turn smoothly by velocity boundary conditions, also of magnitude v_i, but directed tangentially to an arc with radius of curvature equal to $R' = 0.225$, which is the depth of the subduction zone region. Other boundary conditions include free-slip along the top surface and pinned nodes along the boundary with the overriding upper continental plate (Figure 6.2). By enforcing vertical flow along the boundary with the lower continent, we direct flow within the subduction zone and also generate flow within the lower continent region, preventing cold material from accumulating there. This set of boundary conditions for the subduction zone generates stable subduction that can be implemented indefinitely, as long as the thickness of the thermal boundary layer does not exceed that of the subduction zone region.

We must choose the speed, v_i, with which we force subduction to occur. Because the oceanic plate is strong, forcing subduction at a speed v_i causes the plate velocity, v_p to be equal to v_i. To generate convection that is fully dynamic, but that still
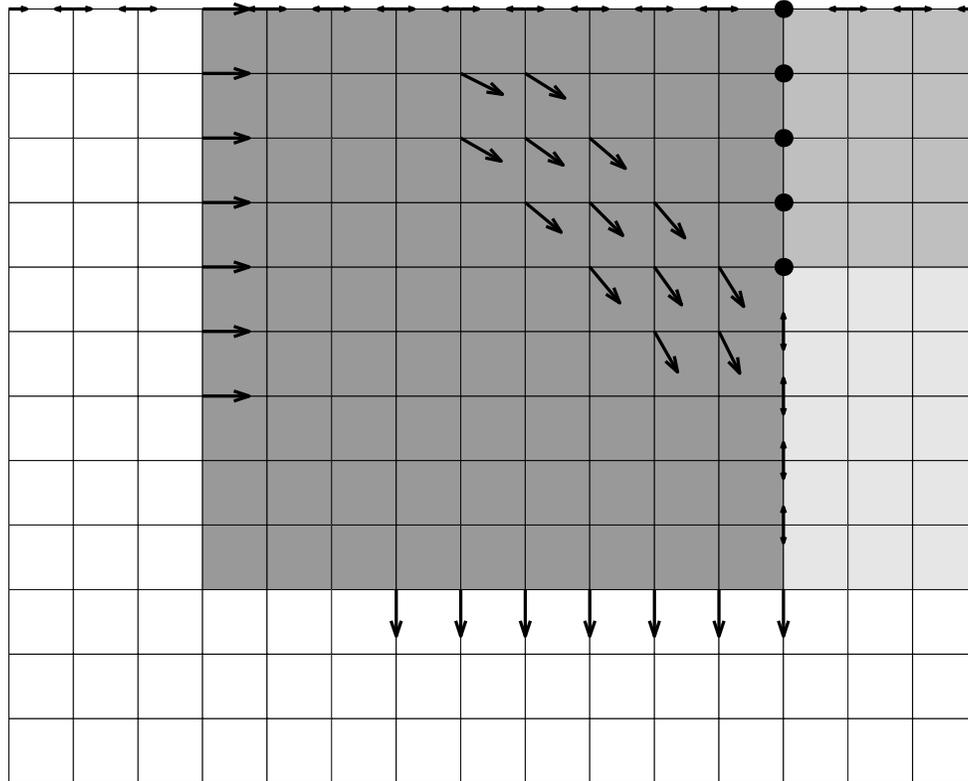
●   Pinned Node

→   Imposed Velocity, v_i

↔   Free Slip

Figure 6.2: A detail of the subduction zone region of the finite element grid showing the velocity boundary conditions used to implement subduction. The large dots indicate pinned nodes and double-sided arrows indicate free slip boundaries. Large arrows indicate the direction of the imposed velocity boundary conditions, which force subduction with a realistic geometry and produce a realistic thermal structure for the resulting slab. All of the imposed velocities have the same amplitude v_i, which is determined by the iterative procedure described in the text.

includes the proper amount of dissipation within the subduction zone, we require the total energy dissipated viscously to be equal to the total potential energy released. Thus, we choose v_i so that $\Phi^{\mathrm{pe}} = \Phi_m^{\mathrm{vd}} + \Phi_l^{\mathrm{vd}}$, which, using (6.2), (6.6), and (6.7) gives:

$$v_p = v_i = \frac{C'^{\mathrm{pe}}}{C_m \eta_m + 2\eta_l \left(h_s/R\right)^3} \tag{6.14}$$

This expression gives the speed with which to drive subduction in order for the subduction zone to dissipate the prescribed amount of energy. To use this expression, however, we must know C_m and C^{pe}, which are not easily estimated for a potentially complicated flow pattern. Because the dependence of C_m and C^{pe} on v_p is weak, we can estimate these quantities by first forcing the system with a chosen velocity v_{i-1}, measuring Φ_m^{vd} (excluding the subduction zone) and Φ^{pe} using (6.3) and (6.1), and then applying (6.2) and (6.6). Applying these estimates for C_m and C^{pe} to (6.14) yields a new expression for v_i that depends on v_{i-1}:

$$v_p = v_i = \frac{\Phi^{\mathrm{pe}}/v_{i-1}}{\Phi_m^{\mathrm{vd}}/v_{i-1}^2 + 2\eta_l \left(h_s/R\right)^3} \tag{6.15}$$

Thus, the proper subduction rate can be calculated using an iterative procedure in which the effects of applying a speed v_{i-1} are tested by measuring Φ_m^{vd} and Φ^{pe} for this speed. A new speed v_i is then calculated using (6.15) and then tested in the same manner. This procedure is repeated until the imposed speed does not change by more than 0.01%. The resulting value of v_i is the rate for subduction that balances potential energy release and the total viscous dissipation, which includes the contribution from the bending slab. This subduction rate is used to advance the flow field by a single timestep, and then is used as the initial test velocity for the next timestep. If the flow field is close to steady-state, convergence occurs in only a few iterations. If the flow field is changing rapidly, convergence typically requires 10 to 20 iterations.

This iteration procedure produces a flow field for which the total potential energy release is equal to the sum of the measured viscous dissipation for the mantle and an expression for the viscous dissipation associated with bending a viscous slab. Thus, it includes, in a dynamically consistent way, the bending deformation of a potentially

strong viscous plate, without requiring the grid resolution necessary to model this deformation accurately. Implementation instead depends on the accuracy of Φ^{pe} and Φ_m^{vd}. We can estimate the error involved with measurements of these quantities by comparing Φ^{pe} and Φ^{vd} for a run in which we do not impose velocity boundary conditions, in which case we expect $\Phi^{vd} = \Phi^{pe}$. For the finite element grid we use, we find that Φ^{pe} is typically greater than Φ^{vd} by up to 2% for $Ra_m \sim 10^5$ and by up to 5% for $Ra_m \sim 10^7$. This difference is associated with errors in the velocity field. Potential energy release depends linearly on vertical velocity, as in (6.1), whereas viscous dissipation depends on the square of velocity in both directions, as in (6.3). Thus, we expect errors in measurements of Φ^{vd} to be larger than those for Φ^{pe}. This is indeed what we find in tests; measurements of Φ^{pe} converge more rapidly with increasing grid resolution than do measurements of Φ^{vd}. Because our measurements of Φ_m^{vd} are slightly too small, our method of forcing the viscous dissipation to balance the potential energy release causes too much viscous dissipation to be placed in the bending lithosphere. This overestimate could be up to 5% for Rayleigh numbers close to 10^7, which are the least resolved of our calculations.

6.3.4   Implementation of the Subduction Zone

To implement this iteration procedure, we modified the finite element code ConMan [*King et al.*, 1990], which calculates the flow velocity field by solving:

$$\mathbf{Ku} = \mathbf{f} \tag{6.16}$$

for $\mathbf{u}$, which is a vector of unknown velocities. Here $\mathbf{K}$ is the "stiffness" matrix, which implements the equations of incompressible Stokes flow for the given finite element grid, and $\mathbf{f}$ is a vector that describes the buoyancy forces that drive the flow. The most time-consuming step in solving for $\mathbf{u}$ is inverting $\mathbf{K}$, an operation that must be performed every time step if the viscosity field changes with time (as it does for temperature-dependent viscosity). Velocity boundary conditions are implemented by removing the specified velocities from $\mathbf{u}$, multiplying them by the associated columns

of $\mathbf{K}$, and then moving the result to the right hand side. Thus:

$$\mathbf{K}_r\mathbf{u}_r = \mathbf{f} - \sum_j u_j\mathbf{k}_j \qquad (6.17)$$

where u_j is the jth velocity boundary condition, $\mathbf{k}_j$ is the jth column of $\mathbf{K}$, the subscript r indicates that rows or columns have been removed, and the summation is over all of the imposed velocity boundary conditions. To change the velocity boundary conditions by a constant factor, as is necessary to update the imposed subduction zone velocity from v_{i-1} to v_i, it is simply necessary to multiply the quantity $\sum_j u_j\mathbf{k}_j$ by the appropriate factor. This method allows the imposed velocity to be updated for each iteration without inverting the stiffness matrix $\mathbf{K}_r$. As a result, the iteration procedure runs quickly and does not add prohibitively to the total computation time.

6.4 Examples of Convection with a Bending Lithosphere

To initiate subduction, we first impose a constant subduction velocity of $v'_i = 500$ on an initially isothermal mantle with temperature $T'_{int} = 0.65$ and Rayleigh number $Ra_m = 10^6$. The cold temperature boundary condition at the surface cools the fluid there and the resulting thermal boundary layer is subducted into the mantle interior, forming a slab. Once the temperature field ceases to change significantly with time, it is used as a starting point for runs in which the rate of subduction is dynamically chosen according method described above. For these calculations, an effective viscosity for the lithosphere, η'_l, is chosen so that the viscous dissipation of the bending slab can be calculated from (6.7). To calculate Φ^{vd}_l, we estimate the plate thickness h'_s using the depth of the $T' = T'_{int}\text{erf}(1) = 0.55$ isotherm. This isotherm was chosen because it represents a high temperature that is consistently within the boundary layer, and thus provides a reliable scale for the boundary layer thickness. As described above, we assume a bending radius of curvature of $R' = 0.225$. For each choice of lithosphere viscosity η'_l, we allow dynamically-driven subduction to

proceed until the system has reached an approximate steady-state, which typically occurs after several thousand time steps. Because, as each system evolves, the mantle typically warms slightly, the viscosity there decreases, leading to Rayleigh numbers greater than the initial value of 10^6. For each calculation, we present the final value of Ra_m, calculated based on the average mantle viscosity. Even after the calculation has reached its "steady state," quantities such as the plate velocity v_p' and the subducting plate thickness h_s' continue to change with time, oscillating about some mean value, as is shown for several different values of η_l' in Figure 6.3. Short time-scale variations in the driving buoyancy field, which occur as the slab interacts with the continent or the base of the mantle region, could cause this behavior. In addition, slight variations in the measured value of the plate thickness h_s should have an amplified effect on plate velocity because the bending resistance depends on the cube of h_s, as in (6.7).

As a first example, we apply an effective lithosphere viscosity of $\eta_l' = 500$. A snapshot of convection at thermal steady state (Figure 6.4) features a flow field and a temperature structure that is consistent with rigid plate motions and subduction-dominated flow. This slab originates at the subduction zone (Figure 6.4a) where the velocity boundary conditions generate a smooth flow of the oceanic lithosphere into the underlying mantle (Figure 6.4b). The strength of the surface plate assures a nearly uniform surface speed between the ridge and the subduction zone. The flow field generated within the lower continent region (Figure 6.4b) results from coupling to the downward motion of the subducting slab. This flow is important because it prevents the development of an overly thick continent by constantly removing cold fluid from the continental base. The temperature field (Figure 6.4a) also contains hot upwelling plumes that originate at the bottom boundary layer.

For the relatively weak lithosphere with $\eta_l' = 10$, an average of only 1.1% of the total viscous dissipation occurs as simulated plate bending within the subduction zone (Figure 6.3c). Thus, for weak lithosphere, bending provides little resistance to convection and plate motions. Increasing the lithospheric strength to $\eta_l' = 100$ or $\eta_l' = 500$, however, causes the viscous dissipation associated with bending to increase (Figure 6.3c), which leads to lower plate speeds (Figure 6.3a). The slower plates are
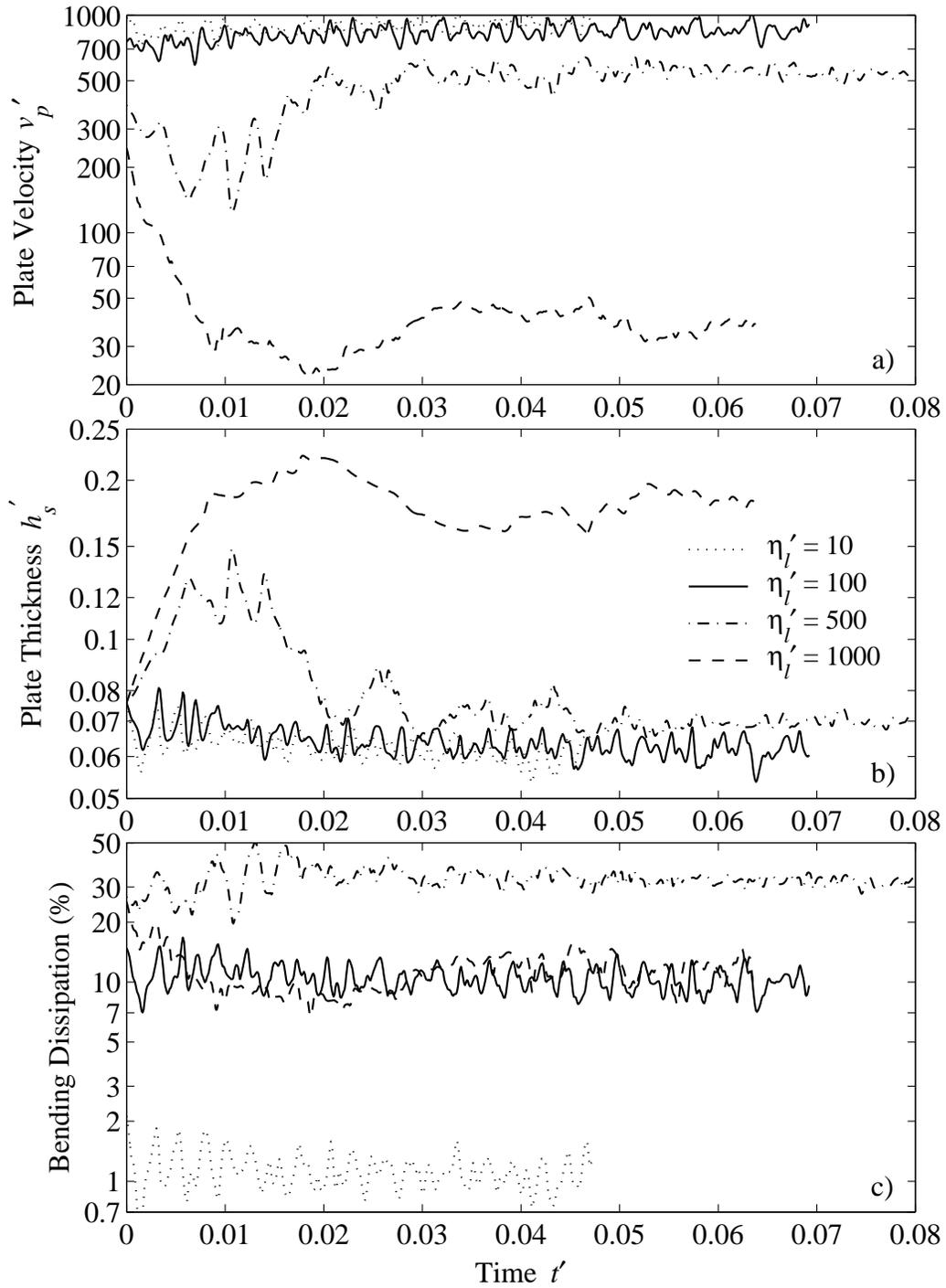
Figure 6.3: A comparison of (a) plate velocity v'_p, (b) plate thickness h'_s, and (c) the fraction of the total energy dissipation that occurs as plate bending within the subduction zone, as a function of time. Results are shown on a log scale for four subducting slabs with η'_l of 10, 100, 500, and 1000, for which Ra_m is 1.1×10^6, 1.2×10^6, 1.5×10^6, and 2.9×10^6.
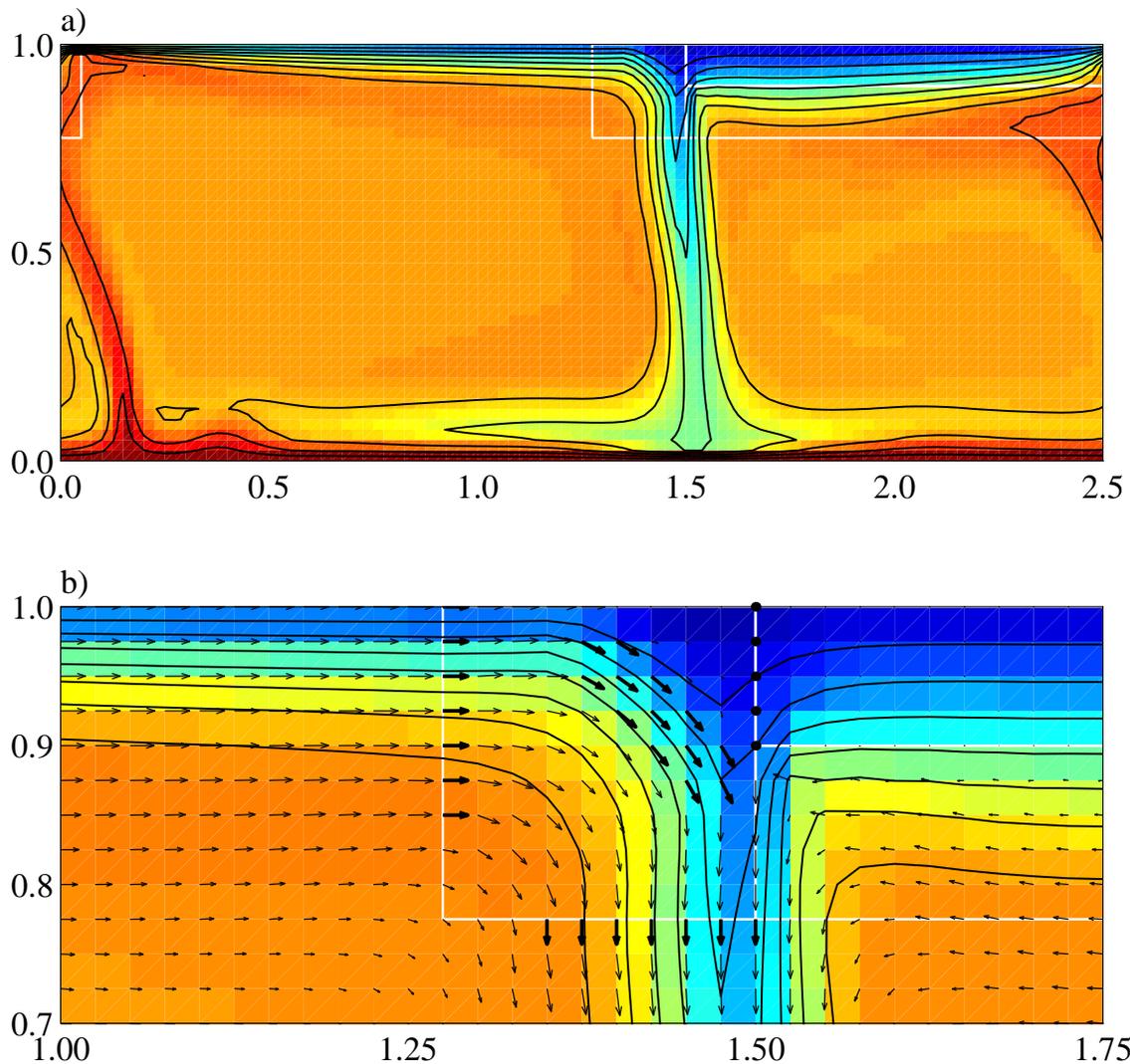
Figure 6.4: A snapshot of convection that includes a bending slab ($\eta'_l = 500$) and $Ra_m = 1.1 \times 10^6$. This combination leads to an average plate speed of $v'_p = 507$ and an average plate thickness of $h'_s = 0.076$. Here, because the slab is weak, only 33.5% of the total viscous dissipation is accounted for by plate bending within the subduction zone; the rest is dissipated viscously in the mantle. The subduction zone, ridge, and upper and lower continents are outlined in white for reference. Denoted by contours in (a) is the temperature field, where the contour interval is 10% of the total temperature variation across the grid. Shown in (b) is a detail of the subduction zone and its surroundings, where the flow field is indicated by arrows. Thick arrows indicate imposed velocities that force fluid through the subduction zone.

slightly thicker (Figure 6.3b) because they have more time to cool as they travel from the ridge to the trench. For a bending slab with viscosity $\eta_l' = 500$, the bending dissipation accounts for 33.3% of the total dissipation (Figure 6.4).

Increasing the plate viscosity still further to $\eta_l' = 1000$ slows the plate significantly (Figure 6.3a), which causes it to thicken. The greater plate thickness increases the bending resistance because Φ_l^{yd} depends on the cube of the plate thickness, as shown by (6.7), and thus leads to a further slowing of the plate. This runaway process rapidly decelerates the plate (Figure 6.3a) and ultimately causes it to thicken by nearly a factor of two (Figure 6.3b). Because the plate motion is so significantly slowed, the deformation occurring within the subduction zone is small compared to that occurring within the underlying mantle, as evidenced by the average bending dissipation of only 10.8% (Figure 6.3c). The temperature and flow fields at steady-state (Figure 6.5) show convection occurring primarily beneath a "stagnant lid." Although a downwelling in the vicinity of the subduction zone is still evident, it involves only the hottest few isotherms and consists of speeds that are much larger than those of the oceanic plate.

Thus, it appears that the total amount of dissipation that can occur within the subduction zone may be limited. If the subduction zone is too strong, surface plates are slowed, and thicken until "stagnant lid" convection develops. We have generated plate-like motions, however, for convection in which 33% of the total viscous dissipation occurs as plate bending within the subduction zone. This is a large fraction of the total and demonstrates that subduction zones can provide significant resistance to convection while still allowing mobile plates at the surface.

6.5   The Temperature Profile of Subducted Slabs

Standard isoviscous boundary layer theory, first applied to the mantle by *Turcotte and Oxburgh* [1967], assumes that convective downwelling is symmetrical, which implies horizontal shortening at the surface. This pure shear representation of downwelling requires the coldest portion of the thermal boundary layer to stagnate at the surface
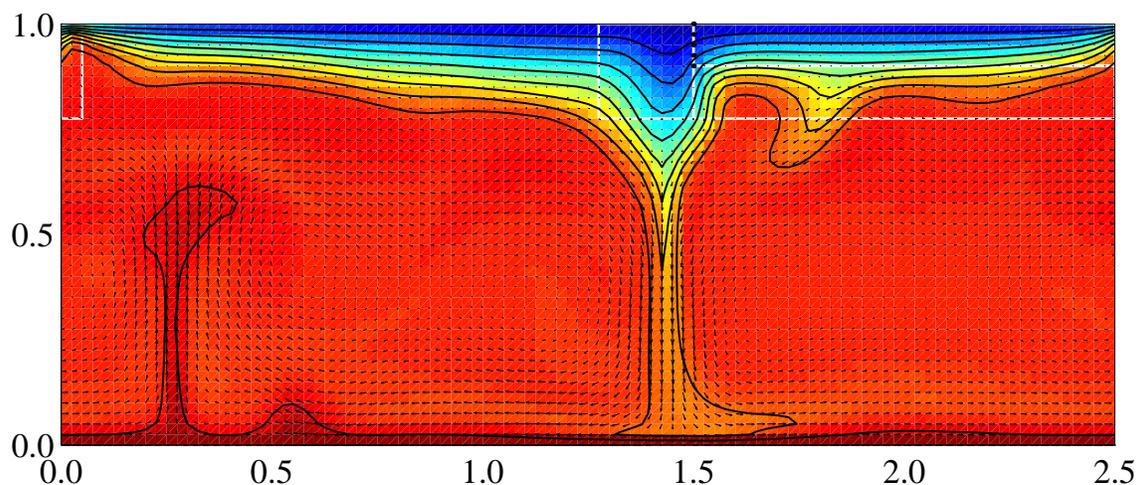
Figure 6.5: Snapshot of convection beneath a "stagnant lid," generated using $Ra_m = 2.9 \times 10^6$ and a slab strength of $\eta'_l = 1000$. As in Figure 6.4, contours indicate temperature and the arrows indicate flow velocities. In this case, the resistance to bending slows the plate, which causes it to thicken and slow further because resistance to bending is greater for thicker plates. This runaway process decelerates the plate to $v'_p = 37$ and produces a bending dissipation of only 10.8%. The subsurface flow velocities, however, are greater and indicate that convection is occurring beneath a "stagnant lid."

above the downwelling. Subduction, on the other hand, is characterized by simple shear along a plate bounding fault, making it inherently asymmetrical. This style of subduction allows the entire thermal boundary layer to participate in convection, which should generate slabs that are colder, and thus more negatively buoyant, than slabs produced by a pure shear mechanism. Here we implement subduction with a set of velocity boundary conditions that were designed to efficiently move the entire thermal boundary layer into the mantle interior. The resulting slabs should thus be colder than slabs produced by methods that require pure shear deformation at the surface.

To demonstrate this point, we compare our implementation of subduction to a pure shear implementation in which we treat the subduction zone as a "weak zone" by removing the velocity boundary conditions and imposing a constant, but low, viscosity of $\eta'_{wz} = 1$ in the subduction zone region. The slab that forms (Figure 6.6)
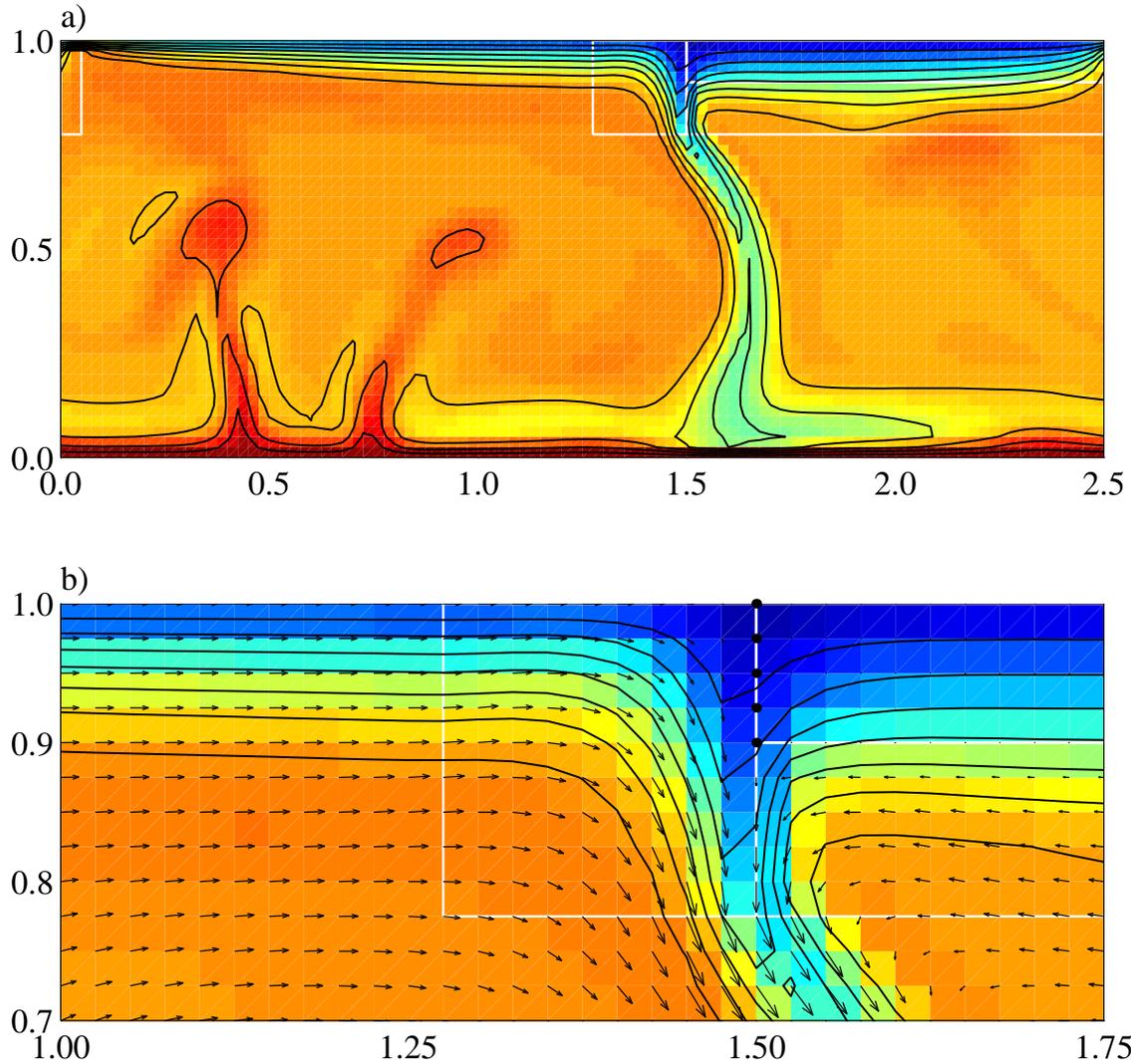
Figure 6.6: Similar to Figure 6.4, but for a "weak zone" representation of subduction and for $Ra_m = 1.4 \times 10^6$. To implement a "weak zone," the velocity boundary conditions used in the previous implementation of subduction are removed and constant viscosity with a value close to that of the mantle interior (here $\eta'_{wz} = 1$) is imposed within the subduction zone. In this case, subduction occurs symmetrically beneath the edge of the continent, which causes the slab to be thinner and have a smaller temperature contrast than in previous models where the subduction zone geometry is imposed (compare to Figure 6.4). Here we find a plate velocity, $v'_p = 496$, and a plate thickness, $h'_s = 0.077$, that are about the same as what we found for a bending slab in which $\eta'_l = 500$ (Figure 6.4), but the viscous dissipation within the "weak zone," here 9.6% of the total, is significantly smaller.

209

has a smaller temperature contrast than does the slab that arises from an imposed subduction zone geometry (compare to Figure 6.4). The difference in thermal structure is more apparent in a cross-section of temperature taken through the base of the subduction zone (Figure 6.7), which shows that a slab formed using a "weak zone" is thinner and warmer than a slab formed with either a strong ($\eta_l' = 500$) or a weak ($\eta_l' = 10$) bending slab. We attribute the decreased negative buoyancy of slabs produced by a "weak zone" to the decreased efficiency with which pure shear moves cold fluid from the boundary layer into the mantle. For the "weak zone," fluid near the surface moves downward more slowly than does deeper fluid, causing subduction to be dominated by the hotter material at the base of the boundary layer. Because the cold surface material does not participate as extensively, the resulting slab is warmer.

We also compare the temperature profiles of the slabs produced here to the profiles expected for the Earth (Figure 6.7). To do this, we measure temperature as a function of horizontal distance using the temperature contours of *Ponko and Peacock's* [1995] detailed models of a slab's thermal structure. We make this measurement at a depth of 200 km depth because this depth is about twice that of the base of the oceanic plate, and is thus analogous to the depth of the previously-plotted profiles in Figure 6.7. To compare temperature profiles, we scale horizontal distance by the approximate thickness of the oceanic plate, which is about 100 km for *Ponko and Peacock's* [1995] results and about 0.1 in Figure 6.4. We also scale the 1300° and 1400°C temperature variation in *Ponko and Peacock's* [1995] models to the corresponding temperature variation of $T' = 0.7$ in our models. The resulting temperature profiles (Figure 6.7) match the profiles for both the weak and strong bending slabs better than they match the profile for the "weak zone" subduction model. Thus, our method for implementing subduction by imposing its geometry produces a realistic temperature profile for the subducted slab, and, as described above, this slab has greater negative buoyancy than slabs produced using only a "weak zone."
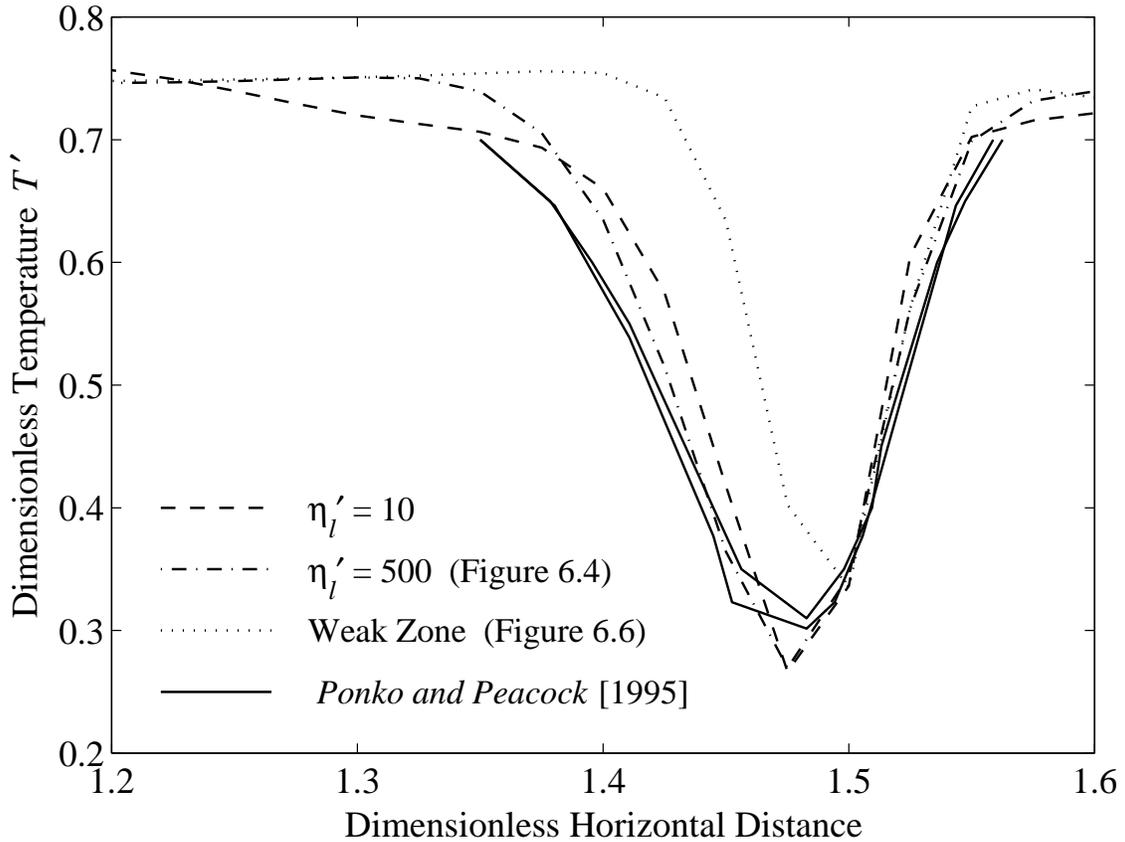
Figure 6.7: A comparison of temperature profiles through the slab for different implementations of subduction, measured in each case at the depth of the base of the subduction zone region. The temperature profile is similar for the weak ($\eta_l' = 10$, dashed line) and the strong (Figure 6.4, $\eta_l' = 500$, dash-dotted line) bending slabs, but the profile for the "weak zone" implementation (Figure 6.6, dotted line) is significantly thinner and warmer. For comparison, we show temperature profiles measured from *Ponko and Peacock's* [1995] two thermal models of the slab beneath Alaska (solid lines), which have been rescaled as described in the text to allow a comparison to our results.

6.6 Application to Boundary Layer Theory

Boundary layer theory, as it is typically applied to the mantle, suggests that increases in the viscosity of the mantle interior should result in slower plate velocities at the surface. We have shown, however, in a few example calculations, that plate velocity may also depend on the viscosity associated with lithospheric bending as a plate subducts. We now investigate how changing the mantle's interior viscosity affects plate velocities for a convective system in which bending of the lithosphere is an important aspect of convection. This analysis can be applied to a cooling Earth, which should experience an increase in its interior viscosity over time.

To vary the mantle Rayleigh number, we apply interior viscosities of $\eta'_{int}(T'_{int}) = 1/3$, 1, and 3. If the average interior mantle temperature were to remain constant at $T' = 0.65$, these choices of viscosity would produce mantle Rayleigh numbers of $Ra_m = 3{\times}10^5$, $1{\times}10^6$, and $3.3{\times}10^6$. Typically, some warming causes Ra_m to increase slightly. Using the same starting temperature field as before, we initiate convection using different lithospheric viscosities η'_l and allow convection to occur until a steady state is reached. At steady-state and for each lithosphere viscosity, we measure the average plate velocity v'_p, plate thickness h'_s, and the fraction of dissipation occurring as bending (Figure 6.8).

Several trends are noteworthy. First, as predicted by boundary layer theory, plate velocity increases with increasing Ra_m (Figure 6.8a), which leads to a thinner oceanic plate (Figure 6.8b). As we found above for a single value of Ra_m, a significant decrease in v'_p (by nearly a factor of two) is observed as the lithosphere viscosity increases from $\eta'_l = 10$ to $\eta'_l = 500$ (Figure 6.8a). This decrease in plate velocity is accompanied by an increase in plate thickness h'_s (Figure 6.8b), and by an increase in the fraction of the total dissipation that occurs as bending (Figure 6.8c). Once lithosphere viscosity increases beyond $\eta'_l = 500$, a stagnant lid develops, as we found above for $\eta'_l = 1000$. The stagnant lid (shown as solid symbols in Figure 6.8) is characterized by much lower plate velocities (Figure 6.8a), exceptionally thick plates (Figure 6.8b), and decreased bending dissipation of less than about 10% (Figure 6.8c).
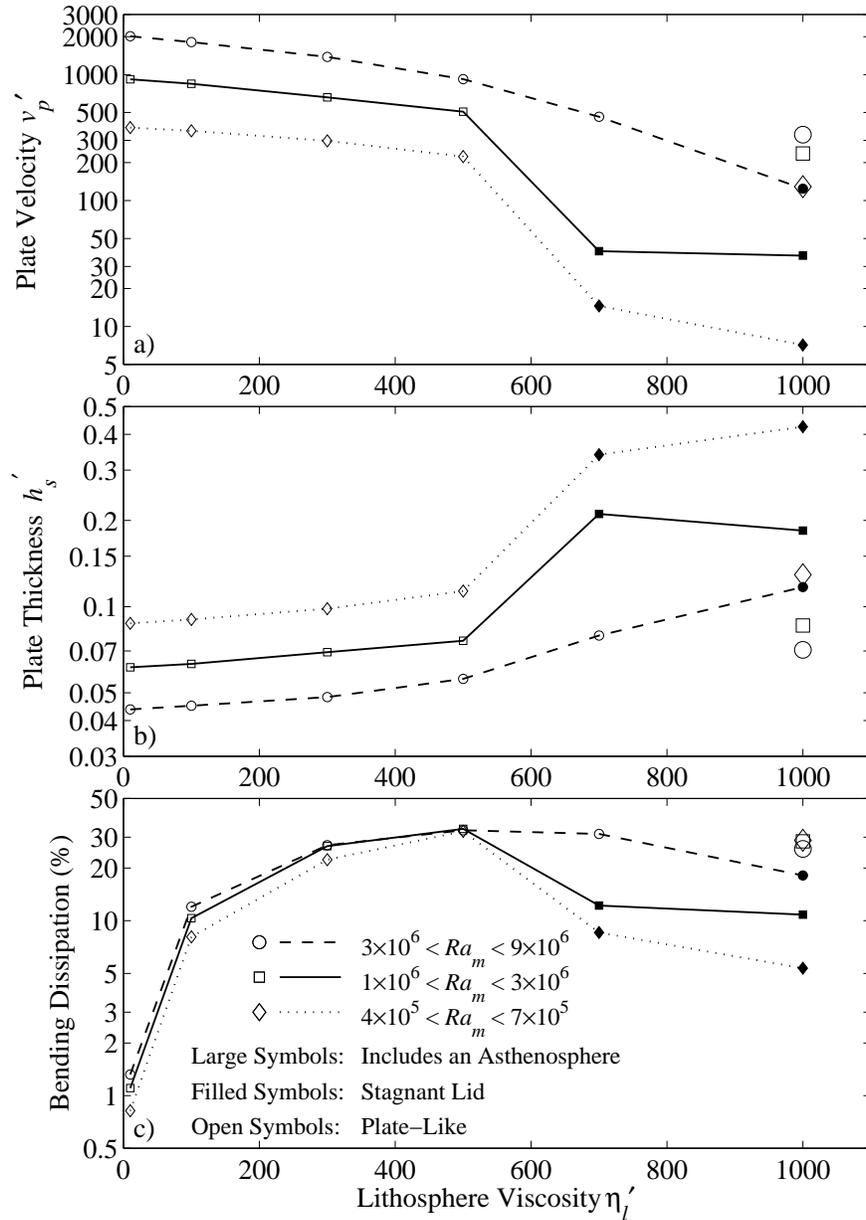
Figure 6.8: The variation of (a) plate velocity v'_p, (b) plate thickness h'_s, and (c) the fraction of the total energy dissipation that occurs as plate bending, as a function of the effective viscosity of the bending plate η'_l. All results are shown on a log scale and the three different lines indicate the grouping of results by mantle Rayleigh number Ra_m. Filled symbols indicate calculations that produce convection beneath a "stagnant lid" while open symbols indicate plate-like behavior. The large symbols denote runs in which a low-viscosity asthenosphere is included, which has the effect of limiting plate thickness and thus preventing the formation of a "stagnant lid." Temperature and flow fields for the three plate-like calculations with an asthenosphere are shown in Figures 6.9 and 6.10.

213

We can compare the trends observed in Figure 6.8 with those predicted by *Conrad and Hager* [1999b], who discuss a variation of standard boundary layer theory that includes viscous bending of the lithosphere at a subduction zone. By balancing Φ^{pe} with Φ_m^{vd} and Φ_l^{vd}, plate velocity v_p can be expressed as:

$$v_p = \frac{\rho g \alpha (T_{int} - T_s) l_s h_s / \sqrt{\pi}}{C_m \eta_m + 2\eta_l \left(h_s / R\right)^3} \tag{6.18}$$

The thickness of a plate at the time of subduction is determined by halfspace cooling, which leads to a relationship between plate thickness and plate velocity of:

$$h_s = 2\sqrt{\kappa L / v_p} \qquad \text{or} \qquad v_p = \frac{4\kappa L}{h_s^2} \tag{6.19}$$

Combining (6.18) and (6.19) yields an expression for plate thickness h_s:

$$h_s = \left(\frac{1}{Ra_m} D^3 \frac{4\sqrt{\pi} C_m Ra_l L / D}{Ra_l - 8\sqrt{\pi} L / l_s} \right)^{(1/3)} \tag{6.20}$$

where, following *Conrad and Hager* [1999b], Ra_l is a "lithospheric" Rayleigh number:

$$Ra_l = \frac{\rho g \alpha (T_{int} - T_s) R^3}{\eta_l \kappa} \tag{6.21}$$

Using (6.19) and (6.20), we can write the relationship between mantle Rayleigh number and both plate thickness and plate velocity in terms of a power-law:

$$h_s \sim Ra_m^{-\beta} D \qquad \text{and} \qquad v_p \sim Ra_m^{2\beta} \kappa / D \tag{6.22}$$

where β is a power-law exponent, given in this case by $\beta = 1/3$. This value for β was originally obtained from boundary layer theory that did not include bending slabs [e.g., *Turcotte and Oxburgh*, 1967], but the above analysis shows that this value should apply even if the bending dissipation is significant. If, however:

$$Ra_l \leq 8\sqrt{\pi} L / l_s \tag{6.23}$$

it is the clear from (6.20) that the plate thickness h_s becomes infinite, in which case the plate velocity v_p approachs zero, and a stagnant lid is formed. This condition occurs when the bending dissipation is sufficiently large such that v_p as expressed by (6.18) is always smaller than v_p expressed by (6.19) [e.g., *Conrad and Hager*, 1999a]. By applying (6.21) to (6.23) and making the lithosphere viscosity dimensionless according to (6.9), we can rewrite the condition for a stagnant lid as:

$$\eta_l' \geq 10^6 \frac{R^3}{D^3} \frac{l_s}{8\sqrt{\pi}L} \tag{6.24}$$

To apply this equation to our model, we set $l_s = D$, $L/D = 1.5$, and $R/D = 0.225$. This yields a condition for the stagnant lid of $\eta_l' \geq 540$, which is independent of mantle viscosity. We observe a transition to a stagnant lid in the range $500 < \eta_l' < 700$ for the two smaller ranges of Ra_m in Figure 6.8, which agrees with theory. For higher Ra_m, the transition occurs at slightly larger η_l', indicating a slight dependence on Ra_m. This deviation from theory may be due to thinning of the oceanic lithosphere by convective erosion at its base, as discussed below.

For lithosphere viscosities smaller than those for which a stagnant lid develops, the fraction of total energy dissipation that occurs as bending is independent of mantle Rayleigh number (Figure 6.8c). This observation can be predicted by first writing an expression for the fraction of dissipation that bending represents, and rewriting this expression in terms of Ra_l:

$$\frac{\Phi^{\mathrm{vd}}}{\Phi_m^{\mathrm{vd}} + \Phi_l^{\mathrm{vd}}} = \frac{2\eta_l h_s^3/R^3}{C_m \eta_m + 2\eta_l h_s^3/R^3} = \frac{2h_s^3}{C_m D^3 Ra_l/Ra_m + 2h_s^3} \tag{6.25}$$

Applying (6.20) to (6.25) yields:

$$\frac{\Phi^{\mathrm{vd}}}{\Phi_m^{\mathrm{vd}} + \Phi_l^{\mathrm{vd}}} = \frac{8\sqrt{\pi}L/D}{Ra_l} \tag{6.26}$$

Thus, the fraction of the total dissipation that bending represents should not depend on Ra_m, but instead on the properties of the lithosphere expressed by Ra_l. This is indeed what we observe; bending dissipation depends more on η_l' than on Ra_m in

215

Figure 6.8c. For lithospheric bending that approaches the "stagnant lid" limit, as defined by (6.23), plates are infinitely thick, so the bending dissipation is 100%. For flow with mobile plates of finite thickness, the maximum bending dissipation should be smaller than this. Here we observe a maximum value of about 33% (Figure 6.8c), which is nearly half of the 50 to 60% value that *Conrad and Hager* [1999a] estimate for the mantle based on the Earth's distribution of surface plate velocities. Their estimate, however, ignores flow beneath continents, which should also be driven by subducting slabs. To include this portion of the flow, the deep mantle portion of *Conrad and Hager's* [1999a] energy budget analysis should be increased by about two thirds, which corresponds to the approximate ratio of continent area to ocean area for the Earth, and also for this analysis. Doing this decreases their estimate of the fraction of bending dissipation to about 35 to 45%, which, interestingly, is consistent with the measurements made here.

6.7   The Role of an Asthenosphere

The resistance to plate bending leads to stagnant lid convection because it slows plate motions, thickening plates and increasing the bending resistance further. This runaway process thus requires the bending resistance to increase as plate motions are slowed, a consequence that can be interrupted in one of two ways. First, various stress-weakening constitutive relations may cause the slab's effective strength to decrease once bending stresses increase beyond a certain point. *Riedel et al.* [1999] suggest that such weakening may place a maximum on the total amount of viscous dissipation that can occur within the bending slab. Once this maximum value is reached, increases in slab age, and thus thickness, do not change the bending resistance, which breaks up the feedback mechanism that leads to a stagnant lid. Another mechanism, proposed by *Conrad and Hager* [1999a, b], could be a process that limits the oceanic plate thickness to some maximum value. In this case, once the oceanic plate thickness saturates, the plate bending resistance would remain constant even for a slab with a Newtonian viscosity.

There is evidence, in fact, that oceanic plates might not achieve their maximum possible thickness at the time of subduction. For example, it has been proposed that plates reach their maximum thickness after about 80 million years, the age at which the linear relationship between seafloor depth and the square-root of its age is observed to break down [e.g., *Parsons and Sclater,* 1977; *Stein and Stein,* 1992]. One mechanism that might limit plate thicknesses is convective erosion at the base of the oceanic lithosphere [e.g., *Davaille and Jaupart,* 1994; *Marquart et al.,* 1999; *Parsons and McKenzie,* 1978], which, if important, would remove cold material below about 100 km, the thickness given by (6.15) for a plate 80 million years old. Convective instability beneath the oceanic lithosphere could be facilitated by the presence of a low-viscosity asthenospheric channel that may exist between 100 and 400 km depth [e.g., *Hager,* 1991]. Although some controversy is associated with the seafloor flattening observation and the mechanism by it occurs [e.g., *Stein and Stein,* 1997], we investigate the effects of limiting the maximum plate thickness by adding a low-viscosity asthenosphere to our calculations.

We introduce an asthenosphere by imposing a constant viscosity with a value $1/10^{\text{th}}$ that of the mantle interior for the 4th through 9th elements from the surface between the ridge and the subduction zone (Figure 6.1). The mantle region above this low-viscosity asthenosphere has temperature-dependent viscosity as before, and therefore continues to behave as a rigid plate. We employ an effective viscosity for bending of $\eta'_l = 1000$, which produces a "stagnant lid" in calculations without an asthenosphere (Figure 6.8), and vary the mantle viscosity as before. The results (Figure 6.8, large symbols), show plate thicknesses that are smaller than is observed for the stagnant lid (Figure 6.8b) and greater plate velocities (Figure 6.8a). Thus, the presence of an asthenosphere facilitates plate-like motion in calculations that would otherwise produce stagnant lid convection.

The velocity and temperature fields produced by these calculations (Figures 6.9 to 6.10) demonstrate how the asthenospheric channel prevents stagnant lid formation. Because the viscosity of the asthenosphere region is smaller than that of the the oceanic plate above it, any cold fluid in the asthenosphere is gravitationally more
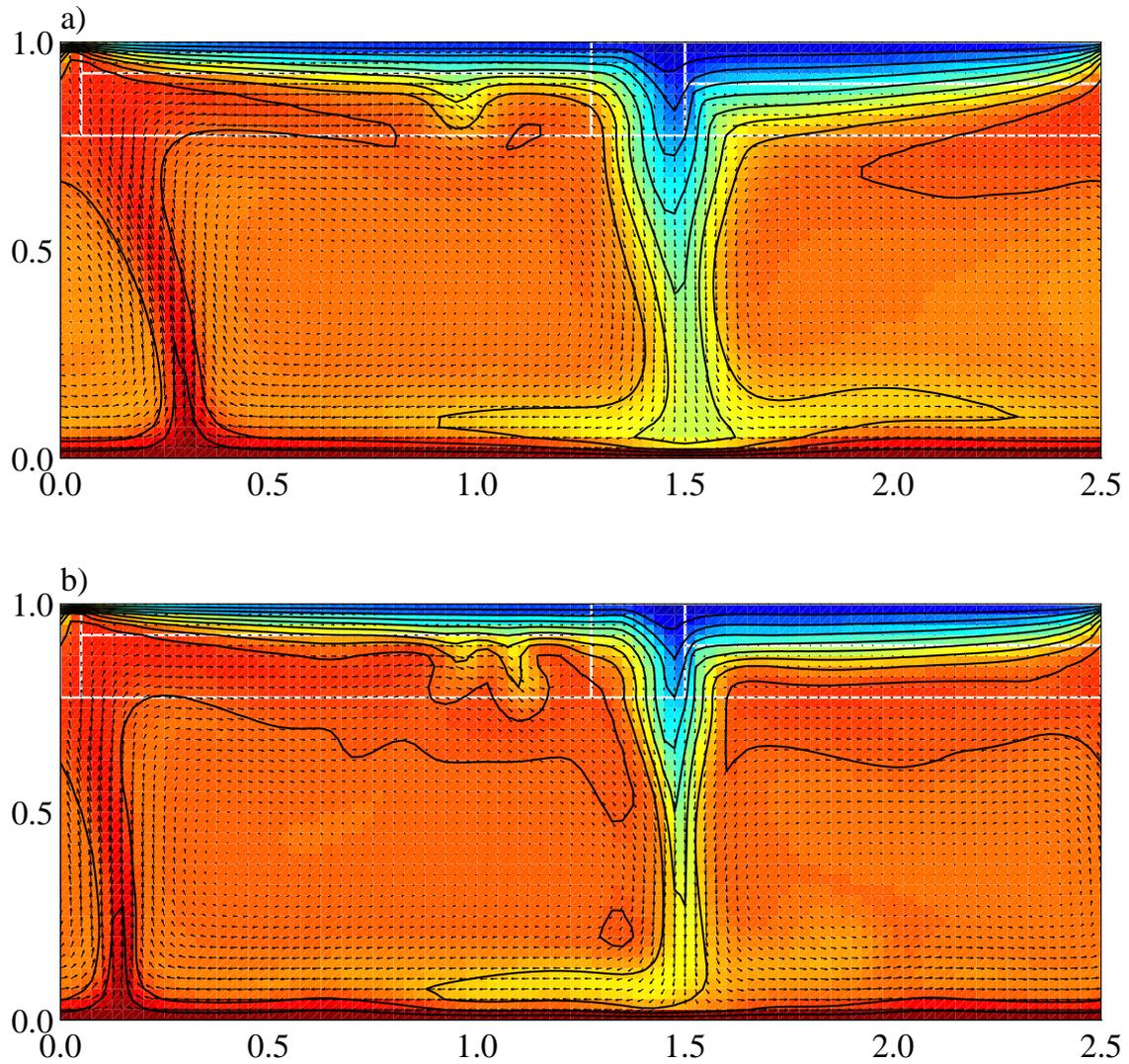
Figure 6.9: Temperature (contours, as in Figure 6.4) and flow (arrows) for convection with a strong bending plate ($\eta_l' = 1000$) and an asthenosphere with constant viscosity that is about $1/10^{\text{th}}$ that of the mantle interior. Shown are results for (a) a mantle Rayleigh number of $Ra_m = 6.4 \times 10^5$ (large open diamond in Figure 6.8) and (b) a mantle Rayleigh number of $Ra_m = 2.1 \times 10^6$ (large open square in Figure 6.8). In both cases, small-scale instability occurs beneath the oceanic plate once it begins to thicken into the low-viscosity asthenosphere. This process removes cold fluid from the base of the plate and limits the thickness to which a plate can grow. Because thick plates cannot form, stagnant-lid convection is averted.

unstable than it is in the overlying plate, and thus can be removed more easily by small-scale convection. The downwellings beneath the oceanic plate in Figures 6.9 and 6.10 demonstrate this process of convective removal of cold fluid from the asthenosphere. Because plates cannot grow thick, slow plates do not become slower because of an additional resistance to bending, and a stagnant lid is avoided. Because, however, the plate viscosity is high, making the bending resistance large, the plates in these calculations move slowly, which permits flow velocities in the interior fluid to to be greater than those of the surface plate (Figures 6.9 and 6.10). This is particularly true at high mantle Rayleigh number (Figure 6.10a), where the rapid removal of the slab once it leaves the subduction zone bears some resemblance to the stagnant lid calculations (Figure 6.5). A detailed look at the subduction zone region (Figure 6.10b), however, shows that surface flow is indeed plate-like. In addition, the deformation of the descending slab that occurs within the mantle is a property of the dependence of slab strength on temperature, a characteristic of slabs that is not well understood and cannot be modeled accurately here. It is possible that a slightly different viscosity law could produce slabs that are strong enough to remain largely intact at high Rayleigh number, despite slow-moving plates at the surface.

If small-scale convection or some other process limits the thickness of plates to some maximum value h_m, the power-law relationships given in (6.22) should apply, but with a value of $\beta < 1/3$. To show this, we note that if $h_s = h_m$, the plate velocity given by (6.18) and (6.19) is no longer relevant. The relative importance of the two terms in the denominator of (6.18) depend on the fraction of dissipation occurring as bending. This can be estimated from (6.25), which, if Ra_m is sufficiently large, shows that the bending resistance should be dominant, even for plate-like flow. In this case, as discussed by *Conrad and Hager* [1999b], the plate velocity, as given by (6.18), depends only on lithosphere viscosity and the buoyancy of the slab, and is thus independent of mantle viscosity and Rayleigh number. As a result, we expect β in (6.22) to be zero.

We test this prediction by measuring the average plate velocity and plate thickness as a function of Rayleigh number (Figure 6.11) for both weak ($\eta'_l = 10$) and strong

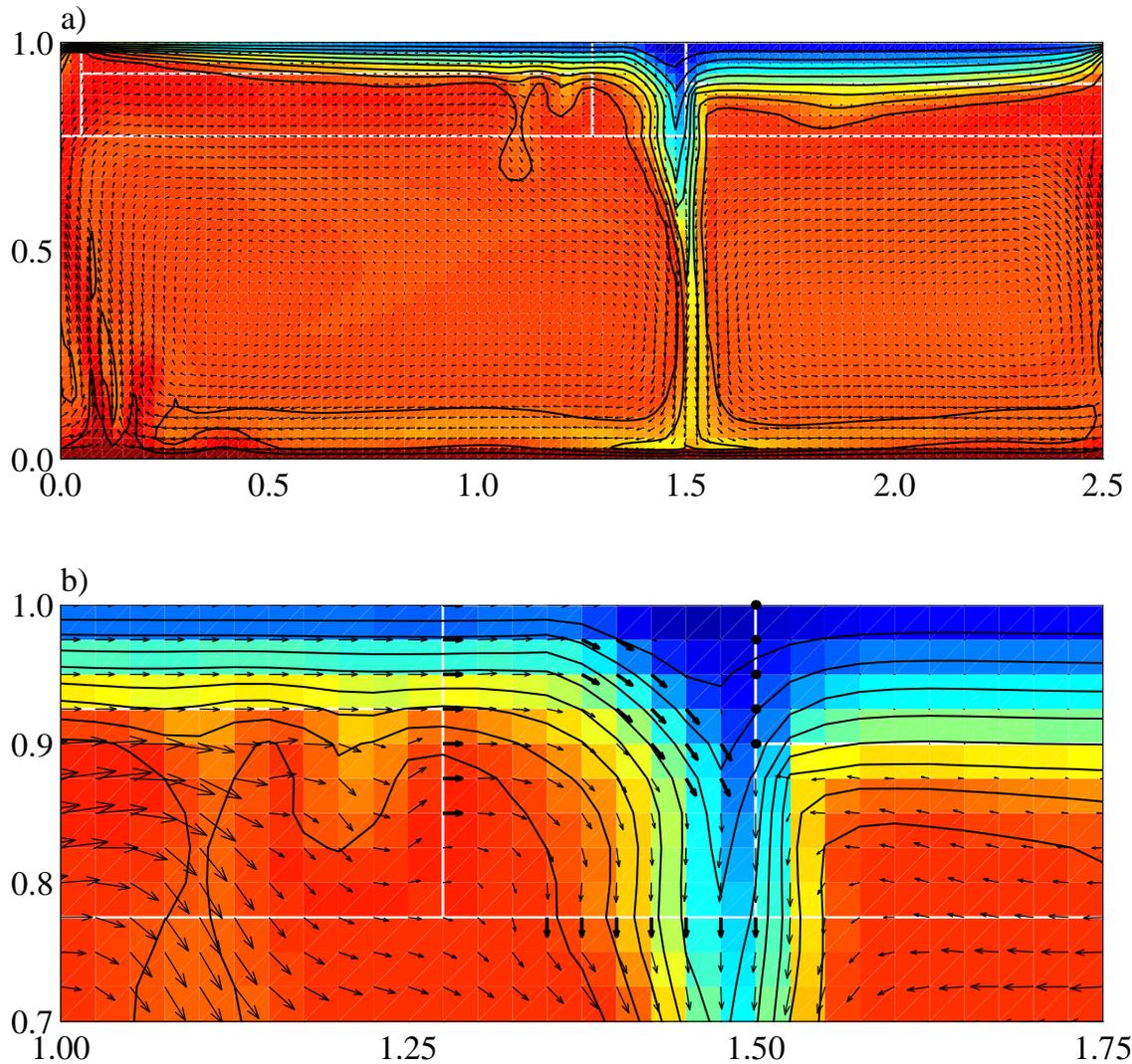Figure 6.10: Similar to Figure 6.9, but for a mantle Rayleigh number of $Ra_m = 8.2 \times 10^6$. The full flow field of convection shown in (a) features some of the attributes of the "stagnant lid" convection shown in Figure 6.5 because the temperature contrast across the downwelling slab is diminished and the flow velocities in the mantle interior are larger than those associated with the plate. The detailed view of the subduction zone region in (b), however, shows that surface motion is, in fact, plate-like. As we found for smaller Rayleigh number in Figure 6.9, small-scale instability removes the basal portions of the oceanic plate and prevents the development of a full-scale stagnant lid.
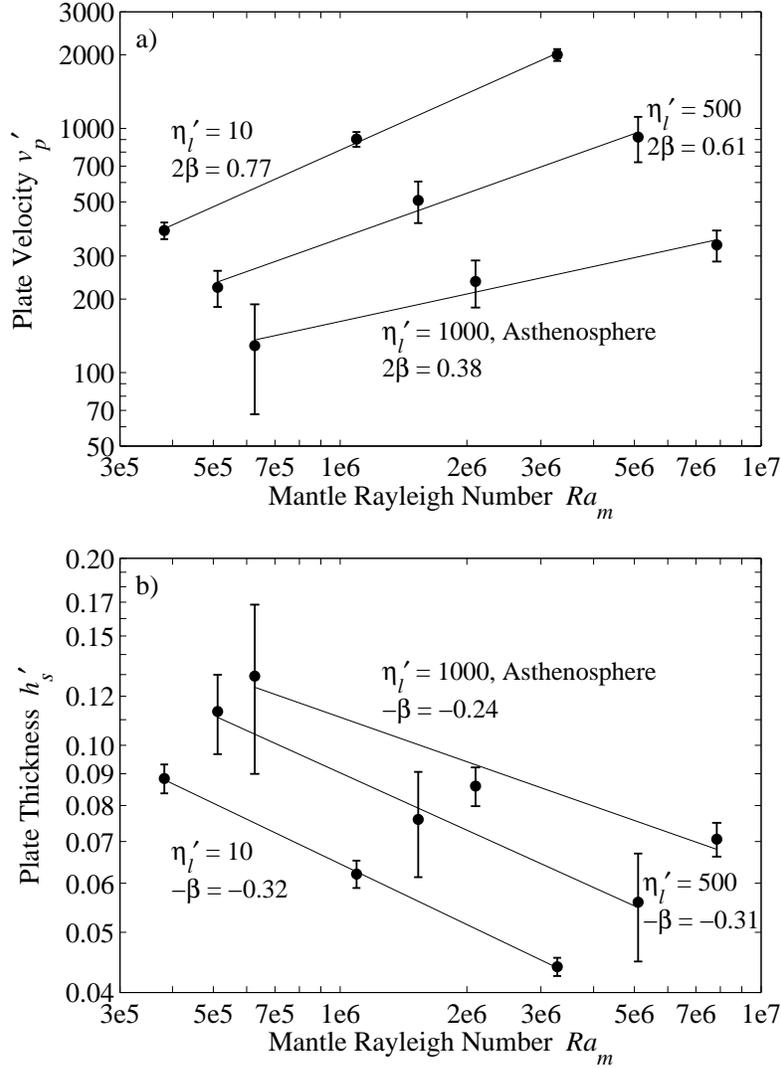
Figure 6.11: Log-log plots showing the dependence of (a) plate velocity v_p' and (b) plate thickness h_s' on mantle Rayleigh number Ra_m. Shown are selected results from Figure 6.8, for a weak bending slab ($\eta_l' = 10$), a strong bending slab ($\eta_l' = 500$), and a strong bending slab ($\eta_l' = 1000$) for a calculation that includes an asthenosphere. As shown in Figure 6.3, both v_p' and h_s' vary significantly with time. Thus, we plot their mean values for the time period after which steady-state has been achieved. Error-bars show one standard deviation from this mean, and thus give an estimate of the uncertainty associated with each measurement. Lines through the points are the least-squares linear fits to the three data points. According to (6.22), v_p' should depend on $Ra_m^{2\beta}$ and h_s' should depend on $Ra_m^{-\beta}$. Thus, we express the best-fit slope of each line in terms of the power-law exponent β, which, if boundary layer theory applies, should have a value of $\beta = 1/3$. The measurements made here indicate that in general $\beta \sim 1/3$, even if the bending resistance is large ($\eta_l' = 500$), but $\beta < 1/3$ for the calculations that include an asthenosphere.

($\eta_l' = 500$) bending plates, and for a strong bending plate with an asthenosphere ($\eta_l' = 1000$). Some uncertainty is associated with these measurements because, as shown in Figure 6.3, both v_p and h_s vary significantly with time, making the measurement of a "typical" value somewhat difficult. As before, we measure an average value at steady-state, but include error-bars with a length of one standard-deviation to show an the approximate range of uncertainty. As predicted, the calculations without an asthenosphere ($\eta_l' = 10$ and 500) produce values of β near $1/3$, even for a strong bending plate. Some variation is observed, but the expected slopes associated with $\beta = 1/3$ could easily fit within the error estimates. The calculation with an asthenosphere, however, shows smaller estimates for β of about 0.19 for velocity and 0.24 for plate thickness. In both cases, calculating a slope using only data from the two larger values of Ra_m would produce an even smaller measurement of β (Figure 6.11). Thus, the addition of an asthenosphere serves to make plate velocity and thickness less dependent on mantle Rayleigh number. Theory predicts a value of $\beta = 0$ if plate thickness is constant. We can see that our implementation of an asthenosphere does not produce constant plate thickness with varying Rayleigh number (Figure 6.11b), which explains measured values of $\beta > 0$ for velocity (Figure 6.11a).

6.8   Heat Flow and the Thermal Evolution of the Earth

The relationship between plate velocities and mantle Rayleigh number has implications for Earth's thermal evolution because this relationship influences the efficiency of convective heat transport. The Earth's primary mechanism for heat loss is the cooling of oceanic plates, for which the total heat flow can be written as:

$$N = 2D \left(\frac{v_p}{\pi \kappa L} \right)^{(1/2)} \sim Ra_m^{\beta} \tag{6.27}$$

which uses the relationship between v_p and Ra_m given by (6.22) [e.g., *Turcotte and Schubert,* 1982, p. 280-3]. Here the heat flow is given by N and is made dimensionless

by dividing by the heat flow expected from conduction occurring alone. Thus N is analogous to a Nusselt number, which measures the efficiency of heat transfer by convection. The response of mantle heat flow to changes in Ra_m is measured by the power-law exponent β, which, as discussed above, should have a value of $\beta \sim 1/3$ if boundary layer theory applies. Thus, as the Earth cools, Ra_m should decrease because the interior mantle viscosity is thought to depend on temperature. If $\beta > 0$, this change should be accompanied by a decrease in N, which slows the mantle's rate of cooling. This negative feedback mechanism has the effect of preventing rapid changes in the temperature of the interior. If β is smaller than the value of $1/3$ predicted by boundary layer theory, this temperature-regulating mechanism is diminished, and more rapid changes in mantle temperature are permitted. Thus, the response of convection to changes in mantle interior viscosity, measured by β, determines the course of Earth's thermal evolution.

The variation of either plate velocity or plate thickness with mantle Rayleigh number (Figure 6.11) produce either measurements of $\beta \sim 1/3$ for subduction zones that are either weak ($\eta'_l = 10$) or strong ($\eta'_l = 500$), but $\beta < 1/3$ for calculations that include an asthenosphere. The value of β applicable for convective heat transfer, and thus for Earth's thermal evolution, can also be estimated directly by measuring the heat flow out of the surface of the finite element calculation. We make this measurement, using the technique developed by *Ho-Liu et al.* [1987], for both the entire grid surface (Figure 6.12a), and for the oceanic plate alone (Figure 6.12b). In both cases, we observe a smaller value of β for calculations that include an asthenosphere. All of the measurements are smaller than the expected value of $\beta \sim 1/3$, presumably because of heat transfer mechanisms that are not associated with the formation of the oceanic plate. Such mechanisms certainly apply for the total heat flow measurement (Figure 6.12a) because a significant fraction of this heat flow occurs as conduction through the continent. This portion of the total heat flow should depend weakly on Ra_m, which explains the smaller measured values of β for the total heat flow (compare Figures 6.12a and 6.12b). Conduction through (as opposed to cooling of) the oceanic plate may occur as well, which could explain the measurements of $\beta < 1/3$

there (Figure 6.12b). Most of the oceanic heat flow, however, occurs close to the ridge where the plate is thin and cooling of the oceanic plate dominates. This portion of the heat flow is related to $v_p^{1/2}$, as in (6.27). For the calculation that includes an asthenosphere, we observe a diminished dependence of v_p' on Ra_m (Figure 6.11a) because the plate velocity is determined η_l' rather than on η_m'. The measurement of $\beta \sim 0.17$ using oceanic heat flow (Figure 6.12b) can be attributed to the same effect.

For a cooling Earth, lithosphere viscosity should depend on surface temperatures, which are thought to have deviated by less than 50°C since the Archean [e.g., *Holland and Kasting,* 1992]. This implies constant lithosphere strength, so if convection rates depend on this strength, plate velocities, and thus mantle heat flow, should be be more constant as the Earth cools than they would be if plate velocities depended solely on the mantle viscosity. Thus, the calculations for which $\beta < 1/3$ predict constant heat flow over time. Small β is not, however, produced by a large bending resistance alone. Instead, the bending resistance must remain constant despite changes in Ra_m, which requires some mechanism for maintaining either constant subducting plate thickness or diminished average strength for thicker plates. As discussed above, either of these two mechanisms are viable possibilities for the Earth.

A diminished value of β has been proposed as a mechanism for explaining an apparent discrepancy between estimates of Earth's current rate of secular cooling and models of the Earth's thermal history that are based on parameterized convective heat transport [e.g., *Christensen,* 1985; *Conrad and Hager,* 1999b]. The former is typically expressed by the Urey number, which is the ratio of mantle's current rate of heat production to its total surface heat flow. This ratio has been estimated to have a present-day value of about 0.5 based on estimates of the concentration of internal heat sources for the primitive mantle [e.g., *Christensen,* 1985]. However, if $\beta = 1/3$, the mantle is efficient at regulating its internal temperature, which implies a small amount of present-day secular cooling. In fact, thermal history calculations suggest that if more than about 15% of the total mantle heat flow represents secular cooling (Urey number of 0.85), a value of $\beta = 1/3$ produces a thermal catastrophe only one or two billion years ago [e.g., *Christensen,* 1985]. If, however, $\beta < 1/3$, the
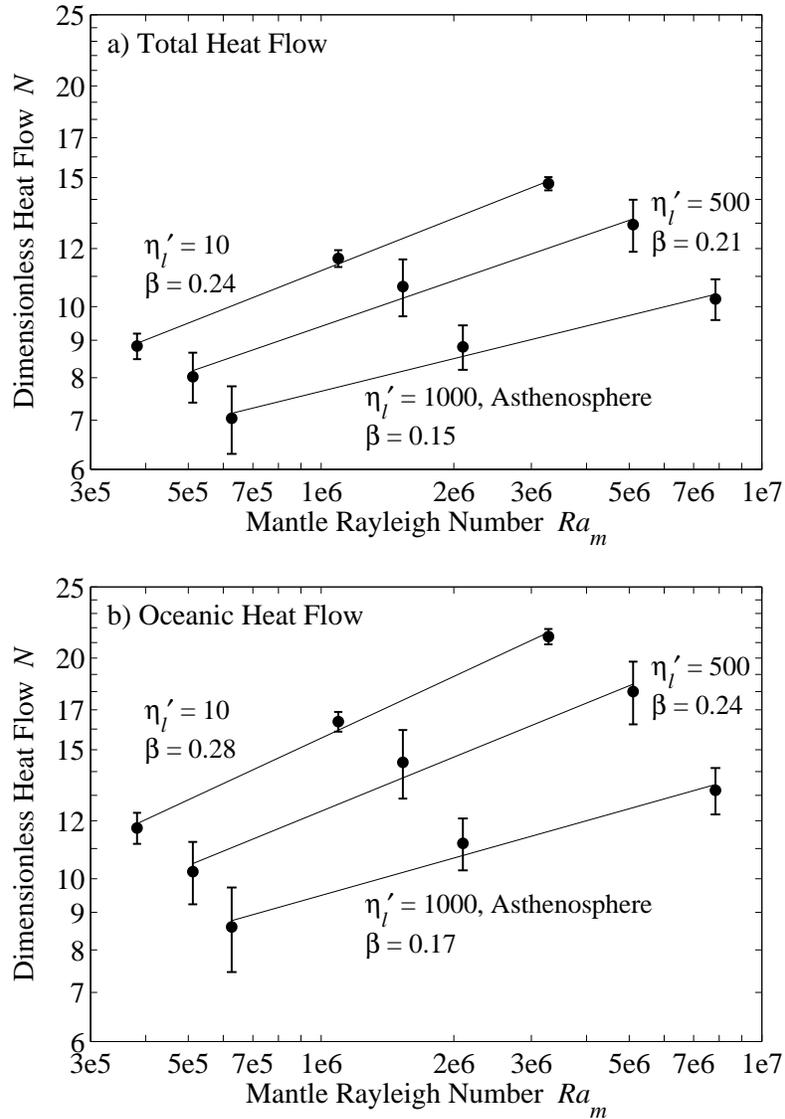
Figure 6.12: Similar to Figure 6.11, but showing measurements of the (a) total heat flow and (b) heat flow out of the oceanic plate, as a function of mantle Rayleigh number Ra_m. Here heat flow is expressed as the dimensionless quantity N, which is normalized by the solution for conduction alone and is thus analogous to a Nusselt number. The slope, β, is measured as shown in Figure 6.11, and boundary layer theory predicts $\beta = 1/3$. This slope is smaller than expected in all cases, but particularly so for the calculations that include an asthenosphere.

mantle is less efficient at regulating its temperature and thus can cool more rapidly, permitting smaller Urey ratios. *Christensen* [1985] estimates that Urey ratios of ~ 0.5 are acceptable if $\beta \sim 0.1$. This is smaller than the estimates of β made here, but it is possible that, as predicted theoretically by *Conrad and Hager* [1999b], Earth-like combinations of mantle Rayleigh number, lithosphere strength, and maximum plate thickness could yield smaller β. Such calculations, however, require computational power beyond the scope of this study.

Christensen [1985] also observed $\beta < 1/3$ in convection calculations that included temperature-dependent viscosity. These calculations, however, pay no special attention to subduction zones, and thus are better described by "stagnant lid" convection without realistic slabs or surface plates. Our model in which plate motions are resisted by lithospheric bending at subduction zones produces Earth-like plate and slab behavior, but still produces decreased β. Other models that generate reasonable subduction by imposing "weak zones" [e.g., *Gurnis,* 1989] do not yield small β because plate velocities depend on mantle viscosity.

6.9   Discussion

The method for implementing subduction developed here incorporates an assumed model for subduction zone deformation into a small region of a finite element grid. Thus, it provides a useful method for incorporating *Conrad and Hager's* [1999b] study of viscous bending for a subducting plate into a larger-scale convecting system without requiring additional numerical resolution. Because this method parameterizes subduction zone deformation using an energy balance, other models for this deformation can also be easily implemented, as long as an expression for the energy they dissipate can be written in terms of the gross physical properties of the subduction zone such as the thickness, velocity and temperature structure of the subducting plate. In particular, it would be useful to study the effects of different rheologies that include stress-weakening or a maximum yield stress.

We enforce a realistic geometry for subduction by imposing velocity boundary

conditions in the vicinity of the subduction zone. As we have shown, this approach produces a more realistic thermal field for the subducted slab than is produced by other methods that employ pure shear at the surface. Using velocity boundary conditions, however, has the disadvantage that the dip angle must be pre-imposed and constant with time. We have found that by using different sets of velocity boundary conditions, subduction with a dip angle smaller than the 90° angle used here can be implemented fairly easily. If an expression for the proper dip angle could be determined from the characteristics of mantle flow, a more fully dynamic representation of subduction could be implemented by imposing the proper set of velocity boundary conditions at each time step. If, however, the velocity boundary conditions change between iterations, the stiffness matrix must be reinverted at each iteration, which would slow the calculation considerably.

Our method for implementing subduction uses an energy balance between viscous dissipation and potential energy release to determine the rate for subduction. Because this energy balance is determined globally, it is unclear how to implement multiple subduction zones. For example, in a model with two subduction zones, some method of dividing the viscous dissipation and potential energy release must be developed so that an expression for the appropriate subduction rate can be determined for both subduction zone. If the flow associated with each subduction zone were independent, then a valid solution could be determined by imposing zero velocity at one subduction zone and using the energy balance method globally to determine the velocity for the other. The velocity for the first subduction zone could be determined by the same method, and then the two velocities could be imposed simultaneously to advance the flow. We would expect an interaction, however, between the flow associated with neighboring subduction zones, so this method might miss some important aspects of convection in a multiple subduction zone system.

Due to computational constraints, we were unable to study Earth-like Rayleigh numbers of $10^7 - 10^8$. Nevertheless, we can apply our analysis to the Earth in several ways. For example, we have found, and theory predicts, that the maximum amount of bending dissipation that can occur before the formation of a stagnant lid, measured

here at 33%, should be nearly independent of mantle Rayleigh number. We have also shown that if some mechanism limits the total bending resistance, stagnant lid convection is replaced by convection with mobile surface plates whose velocity is determined by lithospheric strength. Thus, if such a mechanism is present, the condition for the onset of stagnant lid convection also indicates the onset of convection characterized by plate velocities that are independent of mantle Rayleigh number. This condition, predicted by *Conrad and Hager* [1999b] and verified numerically here, is given by (6.23) as $Ra_l < 8\sqrt{(\pi)}L/l_s$, a condition that does not depend on mantle interior viscosity. For the Earth, we estimate $\rho = 3300$ kg m^{-3}, $g = 10$ m s^{-2}, $\alpha = 3 \times 10^{-5}$ K^{-1}, $T_{int} - T_s = 1300$ K, $\kappa = 10^{-6}$ m^2 s^{-1}, $D = 2500$ km, $R = 200$ km [*Bevis*, 1986; 1988], $l_s = 1000$ km, and $L = 5000$ km. Applying these values to (6.21) and (6.23), we estimate a critical value for the effective lithosphere viscosity of $\eta_l \sim 10^{23}$ Pa s. This estimate is consistent with other estimates of η_l by *De Bremaecker* [1977] and *Conrad and Hager* [1999a] and is a value typically used in studies that generate subduction by introducing faults to strong oceanic lithosphere [e.g., *Zhong and Gurnis*, 1995a, b; *Zhong et al.*, 1998]. Because the mantle's viscosity is temperature-dependent, we expect η_l to be somewhat greater than the viscosity of the underlying mantle. Estimates of the latter are of order 10^{21} Pa s, so an effective viscosity for bending of $\sim 10^{23}$ Pa s is perhaps not unreasonable.

Convection at high Rayleigh number may also have characteristics that cannot be adequately modeled here. In our models, we could implement higher Rayleigh number by decreasing the mantle viscosity. This would induce additional small-scale convection beneath the oceanic lithosphere, even if we did not impose an asthenosphere. Thus, in the Earth, a low-viscosity asthenosphere might not be needed for oceanic plate thicknesses to be limited by convective erosion at their base. On the other hand, decreasing the mantle viscosity in our models would also serve to weaken the downgoing slab. In our lowest viscosity calculations that include an asthenosphere (Figure 6.10), we found that the slab weakens considerably as it descends, causing it to rapidly pull away from the subduction zone. This behavior resembles that of the "stagnant lid," and decreasing the mantle viscosity further might cause the slab to

fall away from the subduction zone altogether. Certainly both small-scale convection and the deformation of a downgoing slab are complicated processes that, like plate bending in subduction zones, depend on the details of the rheology that affect them. We expect that neither is adequately modeled in these calculations, but that both should be essential aspects of the style of convection studied here.

6.10   Conclusions

The method developed here for implementing subduction in a numerical model of convection parameterizes the deformation of a subduction zone within a small region of a finite element grid. Because we do not attempt to model this deformation accurately, but instead rely on more detailed local models to do this, we can easily investigate the effects of different types of subduction zone deformation on mantle flow. To demonstrate the importance of subduction zones to convection, we implement a model for bending a viscous plate within the subduction zone. In particular, we study convection in which oceanic plates maintain their strength as they deform within the subduction zone. This type of "strong" subduction zone cannot be investigated using standard methods for implementing subduction because these methods typically require convergent plate boundaries to be weak.

Using this method, we have shown that plate-like surface motions are produced even if the bending deformation associated with subduction dissipates 33% of the mantle's total convective energy, in which case plate velocities are slowed significantly. Once the bending dissipation reaches this level, plates are slowed sufficiently that they become old enough, and thus thick enough at the time of subduction, that the bending resistance stops plate motion altogether, causing convection to occur beneath a "stagnant lid." If, however, some process prevents the bending resistance from increasing with plate age, plate-like convection can be maintained. One such process could be small-scale convection beneath old oceanic lithosphere, which could limit the thickness to which plates can grow, and thus prevent old plates from becoming too thick to subduct. Various stress-weakening rheologies may also be able to weaken

the subducting slab if it begins to become too thick. Whatever process is involved, it could be an essential aspect of mantle convection that facilitates plate-tectonic motions at the Earth's surface, and thus enables Earth to avoid the "stagnant lid" convection that might apply for Venus or Mars.

If the bending resistance saturates to some constant maximum value, the effective lithosphere viscosity that applies for plate bending should largely determine the velocity of plates. We have shown that, for the Earth, an effective lithosphere viscosity of 10^{23} Pa s should be sufficient to control plate velocities. If this viscosity remains constant despite the increases in mantle interior viscosity that we expect for a cooling Earth, plate velocities, and thus mantle heat flow, should change little over time. Because convection rates are not determined by the mantle interior viscosity, the temperature-regulating feedback mechanism that slows convective heat transfer as the Earth cools is diminished. Thus, an Earth with "strong" subduction zones should experience more rapid changes in temperature, which is consistent with geochemical evidence that about half of present-day mantle heat flow represents secular cooling. As a result, we conclude that the deformation associated with plate bending at subduction zones could be an essential aspect of mantle convection, particularly if the lithosphere remains strong as it subducts. Not only might this additional bending resistance slow plate motions, but it could control the efficiency of convective heat transport, and thus determine the thermal evolution of the Earth.